

Master's Thesis

**Simulation of a Hybrid Solar- Adsorption Cooling System with
Integrated Reversible Heat Pump**

from

Kousha Pourramedani

M.Sc. in degree program

Renewable Energy and Data Engineering (RED)

Offenburg University of Technology, Economics and Media

Faculty of Mechanical and Process Engineering

Institute for Sustainable Energy Systems (INES)

2024

1st Advisor: Prof. Dr. –Ing. J. Pfafferott

2nd Advisor: M.Sc. L.Tomas

Statutory declaration

Statutory declaration

I declare under oath that I wrote the Master's thesis presented here independently and exclusively using the specified literature and other resources. The work was not submitted in the same or similar form to any other examination authority to obtain an academic degree.

Offenburg, April 8, 2024

Kousha Pourramedani

Preface

I wish to extend my heartfelt gratitude to my esteemed supervisors, Prof. Dr.–Ing. J. Pfafferott and M.Sc. L. Tomas, for their invaluable guidance and support throughout the course of my work. Special appreciation is owed to M.Sc. M. Buehler and B.Eng. S. Rissmann for their assistance, which greatly contributed to the success of this endeavor.

I would also like to express my sincere thanks to everyone who supported me on this challenging journey, with special acknowledgment to my beloved wife, family, and friends. Their unwavering encouragement and understanding have been my pillars of strength, motivating me to reach this significant milestone in my academic pursuits.

Kousha Pourramedani
Offenburg, April 8, 2024

Table of contents

Table of contents	1
Figures directory.....	3
Tables directory	4
List of abbreviations	5
Abstract.....	6
1 Introduction	6
2 Modeling.....	10
2.1 Modeling of the individual components	11
2.1.1 Solar collector array.....	11
2.1.2 Adsorption chiller	14
2.1.3 Reversible heat pump.....	18
2.1.4 Dry cooler / Outdoor coil	21
2.1.5 Thermal storages.....	22
2.1.6 Heat Exchangers	26
2.2 Modeling of the Operation modes	27
2.2.1 Cooling modes.....	27
2.2.2 Heating modes.....	29
3 Simulation and results.....	31
3.1 Cooling via adsorption chiller	32
3.2 Cooling via compression chiller + Heating via solar collectors	36
3.3 Heating via solar collectors	39
3.4 Heating via outdoor coil.....	43
4 Summary and outlook	45
Bibliography.....	47
Appendix	48
Data flow diagrams of individual components in SHAKK:.....	48

Thermal storage graphs in simulated operation modes	50
Solar Keymarks data sheet.....	53
Reversible heat pump datasheet	55
Reversible heat pump operation limits:	55
Data used for training of the heat pump's regression model:	56
Data used for training of the compression chiller's regression model:	57

Figures directory

Figure 1.1 - SHAKK system installed at INES	7
Figure 1.2 - System diagram [source: internal].....	8
Figure 2.1 - Flow of data in individual operation modes	11
Figure 2.2 - Arrangement of the Mega Collector modules in SHAKK system [source: internal]	12
Figure 2.3 - Evacuated tube solar collector schematics ^[7]	13
Figure 2.4 - mechanical vs. thermal cooling ^[12]	15
Figure 2.5 - Schematics of the operation of an adsorption chiller ^[12]	16
Figure 2.6 – schematics of a basic adsorption cycle (top) vs. a two-bed continuous adsorption cycle (bottom) ^[13]	17
Figure 2.7 - Energy flow of adsorption chiller	18
Figure 2.8 - Energy flow in the compression chiller	19
Figure 2.9 - Energy flow in the heat pump.....	20
Figure 2.10 - Sketch of a dry cooler ^[12]	21
Figure 2.11 - Schematics of the thermal storage unit	24
Figure 2.12 - schematics of the system under cooling via adsorption chiller mode	28
Figure 2.13 - schematics of the system under cooling via compression chiller mode	28
Figure 2.14 - schematics of the system under heating via solar collectors' mode	29
Figure 2.15 - schematics of the system under heating via outdoor coil mode	30
Figure 3.1 - Schematics of the data flow in cooling via the adsorption chiller operation mode	32
Figure 3.2 – Irradiance and temperature changes during the day 10.6.2022	33
Figure 3.3 - Temperature changes in the solar collectors	33
Figure 3.4 - Adsorption chiller's temperature changes	34
Figure 3.5 - Adsorption Chiller's COP changes	35
Figure 3.6 - Schematics of the data flow in cooling via the compression chiller operation mode	36
Figure 3.7 – Temperature changes in the solar collectors	37
Figure 3.8 - Compression chiller's temperature changes	38
Figure 3.9 - Compression Chiller's COP changes	39

Figure 3.10 - Schematics of the data flow in heating via the solar collectors' operation mode	39
Figure 3.11 – Irradiance and temperature changes during the day 27.2.2022	40
Figure 3.12 - Temperature changes in the solar collectors	41
Figure 3.13 – Heat pump's temperature changes	42
Figure 3.14 - Heat pump's COP changes	42
Figure 3.15 - Schematics of the data flow in heating via outdoor coil operation mode	43
Figure 3.16 - Heat pump's temperature changes	44
Figure 3.17 - Heat pump's COP changes	44

Tables directory

Table 2.1 - Constant values in Eq.2-2.....	14
Table 2.2 - regression coefficients of the compression chiller model	20
Table 2.3 - regression coefficients of the heat pump model.....	21
Table 2.4 - Outdoor coil parameters	22
Table 2.5 - Thermal storage parameters.....	23
Table 2.6 - governing equations in thermal storage units	25
Table 2.7 - Parameters and Equations for Thermal Storage Modeling	25
Table 2.8 - Parameters of the heat exchangers.....	26
Table 3.1 - volume flow rates values in between components.....	32
Table 3.2 – volume flow rates values in between components	37
Table 3.3 - volume flow rates in between components	40
Table 3.4 - volume flow rates in between components	43

List of abbreviations

AdC	Adsorption chiller
CC	Compression chiller
CSP	Concentrating solar power
ETC	Evacuated-tube collector
FPC	Flat plate collector
HP	Heat pump
HT	High temperature
HTF	Heat transfer fluid
HTS	High temperature storage
LT	Low temperature
LTS	Low temperature storage
MT	Intermediate temperature
NTU	Number of transfer units
OC	Outdoor coil
POA	Plane of array
RC	Dry cooling tower (recooler)
RHP	Reversible heat pump
SC	Solar collector

Abstract

This thesis explores the feasibility and optimization of a solar-thermal sorption system mainly designed to provide cooling but also capable of heating functionalities. Through the development of a black-box model using Python programming, the study delves into the system's performance under various operation modes. Simulation results reveal the effectiveness of adaptive control strategies and pre-heating stages in optimizing efficiency, particularly in cooling modes. In heating assessments, superior performance is observed when utilizing the outdoor coil as the heat source for the heat pump. Challenges related to operational temperature bands are addressed, proposing parallel connections of the heat pump and outdoor coil to enhance performance. Future research directions include refining regression models and incorporating real-time measurement data for improved accuracy, as well as extending simulation duration for comprehensive evaluations. This study contributes valuable insights into the system's capabilities and applications, laying the groundwork for advancements in heat-driven integrated sustainable energy systems.

Key words: Simulation, Python, Black-box modeling, Regression model, Heating, Cooling, Evacuated-tube solar collector, Adsorption chiller, Compression chiller, Heat pump

1 Introduction

To reduce greenhouse gas emissions and establish an affordable, secure, and reliable energy supply, it is proposed that most of our future energy requirements be generated from renewable sources and that these sources be used efficiently. Worldwide transformation of our energy systems can be achieved through the utilization of sustainable energy solutions. Solar energy, which can be harnessed in diverse forms for generating heat and electricity, is considered an inexhaustible source of energy.

On a related note, the demand for heating often fluctuates seasonally, with lower demand in the summer. Meanwhile, the options for heat production are relatively constant over the course of the year. By appropriate technology implementation

such as sorption chillers, the exploitation of heat surpluses to cover cooling requirements is possible, rather than leaving this energy unused. Its use in year-round applications such as industrial cooling is also feasible^[1].

Introducing SHAKK (Solares Heizen durch Adsorption und Kompression beziehungsweise Kühlen) which is primarily a solar-thermal source heat-driven chiller that is integrated with a reversible heat pump to offer both heating and cooling functionalities. Situated at the Regional Innovation Center for Energy Technology (RIZ) within the Institute for Sustainable Energy Systems (INES) at Offenburg University of Applied Sciences in Offenburg, Germany. In Figure 1.1 pictures taken from the actual installed system can be seen. SHAKK was conceptualized based on principles outlined in the work of Bürger.A et al^[2].



Figure 1.1 - SHAKK system installed at INES

The system comprises several key components, including an array of evacuated-tube solar collectors, an adsorption chiller, a dry cooling tower, a reversible heat pump, and storage units for both high and low temperatures. This innovative setup allows for efficient utilization of renewable energy sources while offering versatile heating and cooling solutions. In Figure 1.2 a schematic diagram of the system provided from the manufacturer is shown.

The primary objective of this study is to develop a black-box model for SHAKK. Black-box models, selected for their reliance on empirical data, are commonly utilized when integrating sorption storage into larger dynamic systems, such as solar cooling systems or multigeneration systems^[3]. These models aim to determine the temperatures within each component and the thermal storage unit by solely utilizing daily weather data, including ambient temperature and irradiance levels.

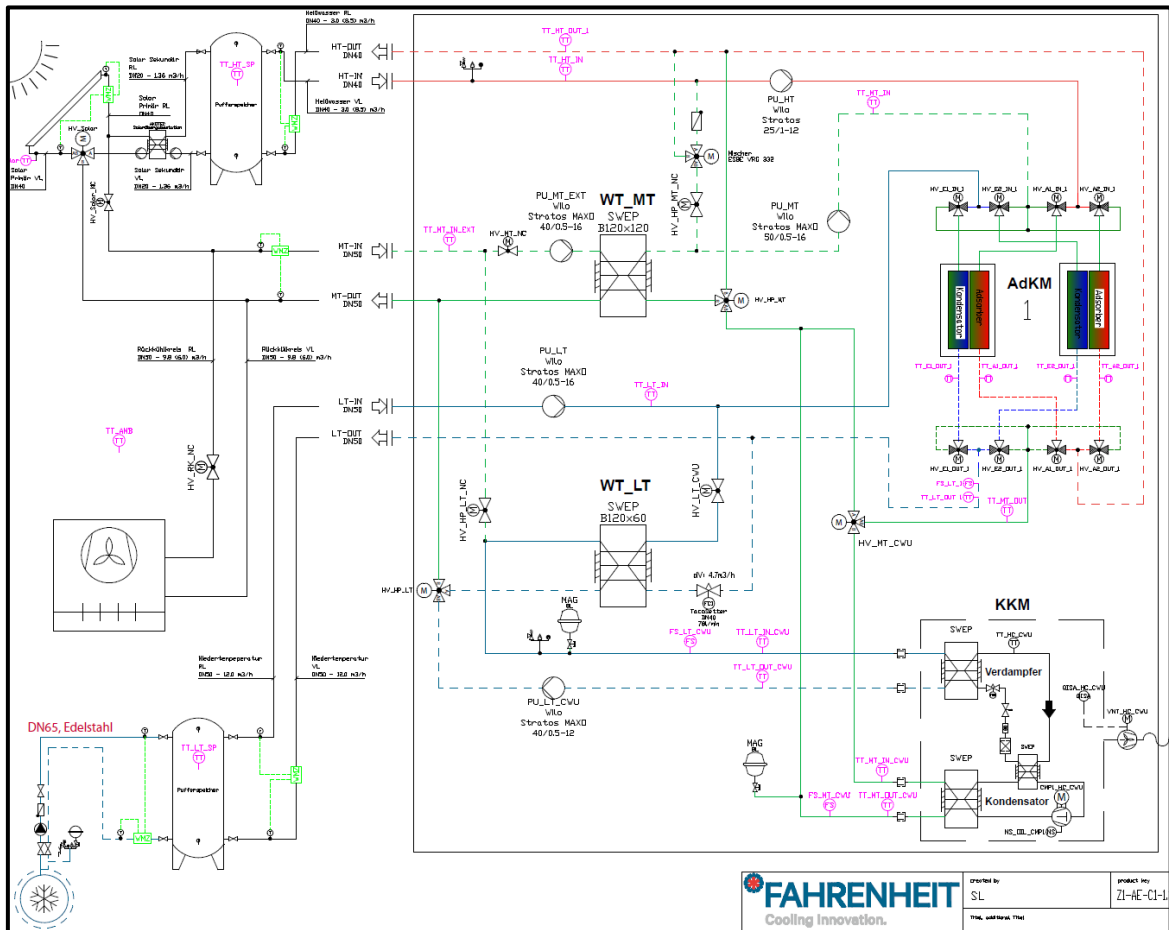


Figure 1.2 - System diagram [source: internal]

The motivation behind this work was to develop a simple basic model so that when combined with actual measurements, this model could become instrumental in fault diagnosis and system optimization. By accurately predicting temperatures and system behavior, it offers valuable insights into system performance and efficiency, facilitating informed decision-making and enhancing overall system reliability.

The modeling process is conducted using the Python programming language. Each component of SHAKK is individually modeled to capture its specific behavior and interactions within the larger system. This approach allows for a comprehensive

understanding of the system dynamics and enables detailed analysis of its performance under various operating conditions.

In the upcoming chapters, a thorough examination of the modeling intricacies, encompassing both the operational modes and individual components of SHAKK can be expected. This section will delve into the nuances of how the system functions under diverse conditions, shedding light on its dynamic behavior and performance attributes. Following this, the simulation results will be unveiled, providing valuable insights into the system's response to various inputs and operating scenarios. Additionally, a comprehensive summary and outlook will be presented, offering a concise recapitulation of the key findings and implications of the study, alongside potential pathways for future research and development in the field. Through these chapters, readers will achieve a comprehensive understanding of SHAKK's capabilities, limitations, and potential applications in sustainable energy systems.

2 Modeling

This chapter is dedicated to the principles of modeling, which serve as the cornerstone of this work. Modeling is regarded as a powerful tool for understanding, analyzing, and predicting the behavior of complex systems, enabling various scenarios to be simulated and system performance to be optimized.

The chapter is structured into two main subchapters, each focusing on distinct aspects of modeling. In the first subchapter the modeling of individual components within the system is examined. Here, the variables, parameters, and operational principles of each component are explored, shedding light on the equations and methodologies used for modeling. The second subchapter, explores the operation modes of the system, providing insights into the different modes of operation and their underlying principles. The goal is to provide a comprehensive understanding of the thermodynamics of the system and how each component contributes to its performance.

Python^[4] served as the primary modeling environment for our work. This programming language is well-suited for scientific computing and data analysis, boasting an extensive ecosystem of libraries and frameworks along with being open-sourced and well documented. For instance, the Scikit-learn^[5] library is employed for the development of regression models for the reversible heat pump, while the PV-lib^[6] library is used for the calculation of Plane of Array (POA) irradiance in the solar collectors.

The goal of modeling is to simulate the system under each operation mode at every time step as closely to reality as possible. Figure 2.1 illustrates the connection between components at each operation mode, as well as the flow of data between them. Starting with weather data at the top, the results of the models are seen in the temperatures at the thermal storage unit at the other end.

In essence, this chapter lays the groundwork for understanding the dynamics of the system. Through modeling and simulation, valuable insights into system behavior are gained, and opportunities for improvement are identified.

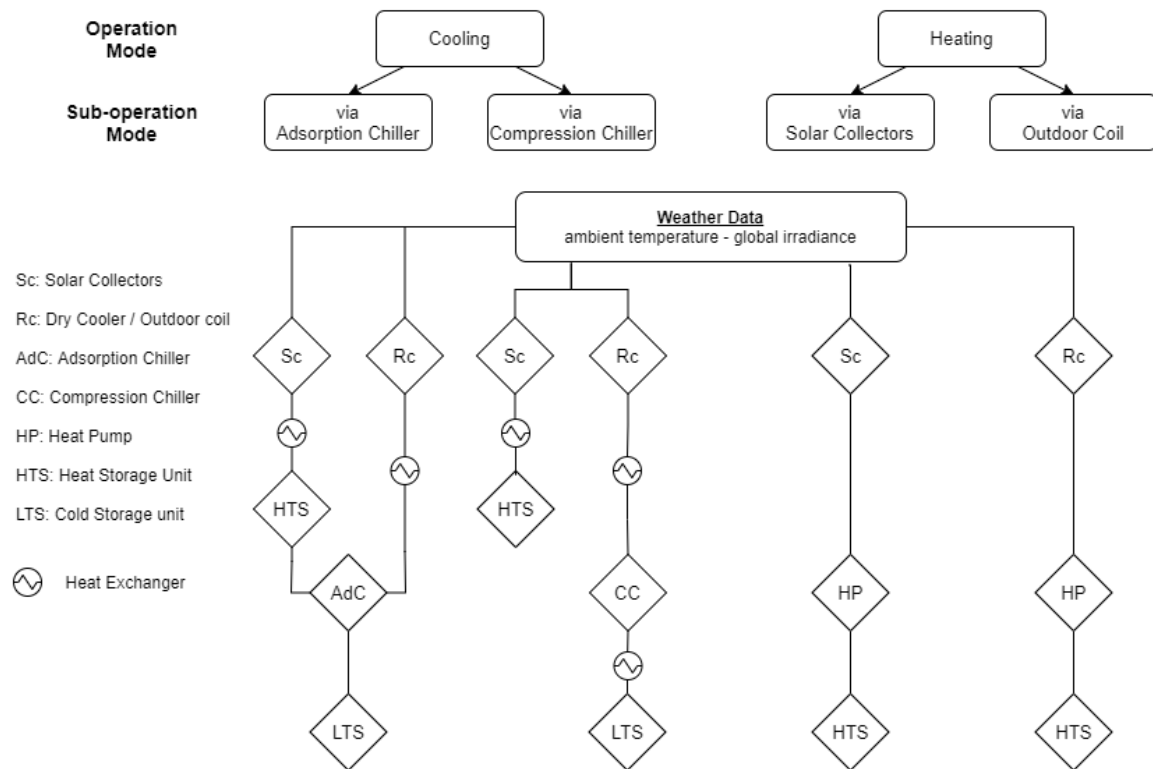


Figure 2.1 - Flow of data in individual operation modes

2.1 Modeling of the individual components

This section is devoted to discussing the modeling of the individual components within the SHAKK system. Here, the aim is to comprehensively explore the variables and parameters associated with each component while providing insights into their operational principles. Through this exploration, the equations utilized in the modeling process will be clarified, offering a deeper understanding of the system's thermodynamics.

2.1.1 Solar collector array

Principle of operation: Solar cooling is an application of solar thermal energy technology specifically designed for cooling purposes. Solar thermal energy technologies can be broadly classified into two main categories: non-concentrating and concentrating. Concentrating collectors, also referred to as concentrating solar power (CSP) technologies, are typically utilized for medium (150–300 °C) and high (>300 °C) temperature applications, providing energy at elevated temperatures and requiring a tracking mechanism for optimal efficiency. These technologies are more suitable for industrial application and fall out of the focus of this work. On the other hand, non-concentrating collectors, exemplified by flat plate collectors (FPCs) and

evacuated tube collectors (ETCs), function differently from CSP. They incorporate a blackened absorbing surface to capture solar radiation, with the absorbed energy transferred to the working fluid flowing inside the absorber tube or channel. These collectors generate low-temperature heat (as high as 120°C) suitable for various applications, including domestic and process heating.

The installed system at INES involves the use 52 m² of ETCs. In contrast to the temperature range of 80–100°C commonly observed in FPCs, evacuated tube collectors boast higher temperatures, specifically ranging from 100 to 120°C. This temperature difference results from effectively reducing heat losses in ETCs by enclosing the absorber tube within a precisely sealed evacuated tube^[9].

Principle of modeling: The collector array consists of four solar mega collector segments manufactured by Akotech GmbH^[7], as illustrated in Figure 2.2. Each segment integrates 78 evacuated tube collectors of HP140 type, interconnected in parallel configuration, as shown in Figure 2.3. Heat pipe (HP140) model has been selected here specially in order to avoid over heating in the collectors under standstill condition. These collector models have the capability to reach stagnation temperatures of up to 140°C. However, to ensure operational safety and efficiency, the control system implements a shutdown when the temperature reaches 97°C.

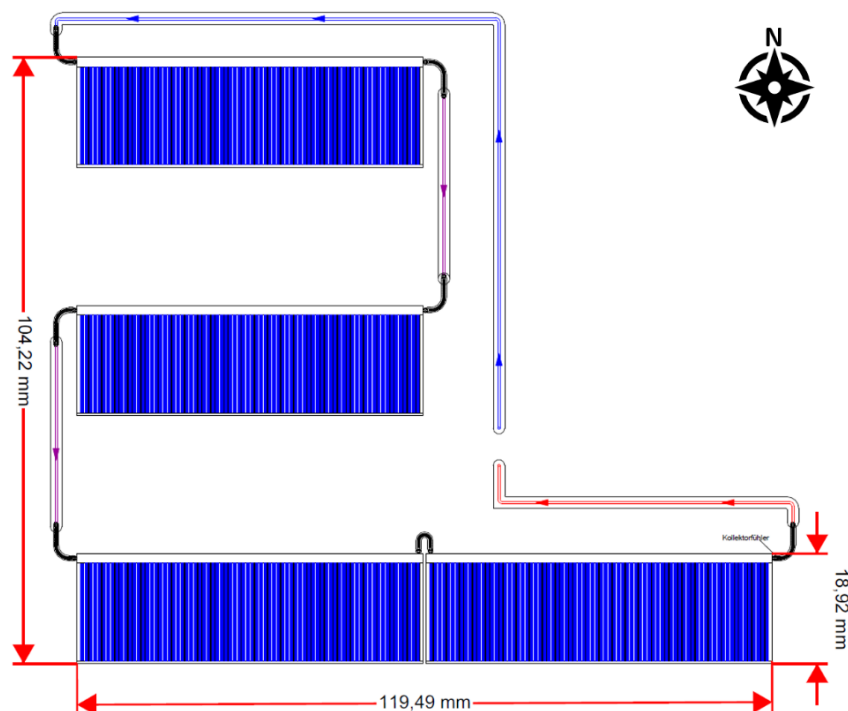


Figure 2.2 - Arrangement of the Mega Collector modules in SHAKK system [source: internal]

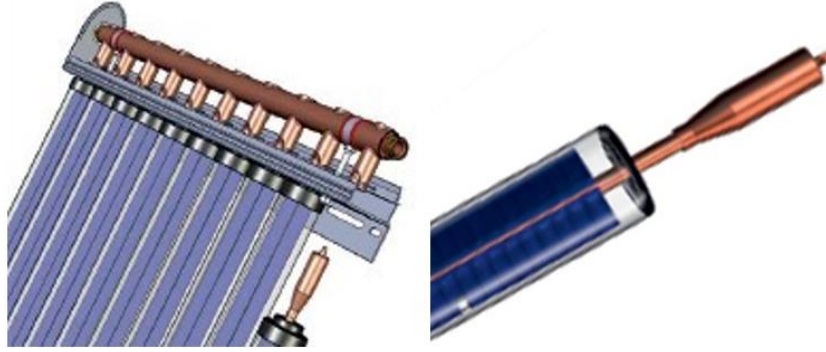


Figure 2.3 - Evacuated tube solar collector schematics^[7]

The calculation of the heat output from a collector is typically based on the ISO 9806:2017 equation^[10,11]. Normally, the first four components of the equation representing the irradiance, diffuse irradiance, heat loss, and temperature dependence on heat loss are considered. However, for a more realistic outcome, the effective thermal capacity of the collector has also been considered into the model. The heat output equation for each mega collector array is given by:

$$\dot{Q} = A_G \left[\eta_{0,b} K_b G_{b,H} + \eta_{0,d} K_d G_{d,H} - a_1 (\vartheta_m - \vartheta_a) - a_2 (\vartheta_m - \vartheta_a)^2 + a_5 \left(\frac{d\vartheta_m}{dt} \right) \right] \quad (\text{Eq.2-1})$$

where A_G represent the gross area of the collector, $\eta_{0,b}$ peak collector efficiency based on beam irradiance $G_{b,H}$, $G_{d,H}$ horizontal plane diffuse irradiance, ϑ_m mean temperature of heat transfer fluid, and ϑ_a ambient air temperature. The coefficients a_1 , a_2 , and a_5 represent the heat loss, temperature dependence of the heat loss, and effective thermal capacity, determined during standard tests and provided in the product's Solar Keymark datasheet of the mega collector which can be found in the Appendix.

Instead of calculating the beam and diffuse irradiance of the horizontal plane and multiply it by incident angle modifier coefficients K_b and K_d , the beam and diffuse irradiance of plane of array can be calculated. here the PV-lib library^[6] has been used to calculated them based on the geographical location, Global irradiance and the positioning of the mount. Additionally, $d\vartheta_m/dt$ can be simplified to $\vartheta_m - \vartheta_{m,prev}/\Delta t$ considering the 1-minute time intervals, due to the high-volume flow rate of the system. Eq.2-1 can be rewritten as:

$$\dot{Q} = A_G \left[\eta_{0,b}(G_{b,poa} + G_{d,poa}) - a_1(\vartheta_m - \vartheta_a) - a_2(\vartheta_m - \vartheta_a)^2 + a_5\left(\frac{\vartheta_m - \vartheta_{m,prev}}{\Delta t}\right) \right] \quad (\text{Eq.2-2})$$

in which $\Delta t = 60_{[s]}$ and $\vartheta_{m,prev}$ is the mean temperature of the previous time interval. The constant values are detailed in Table 2.1.

Table 2.1 - Constant values in Eq.2-2

Parameter	Value	Unit
A_G	12.99	m^2
$\eta_{0,b}$	0.49	-
a_1	0.63	$W/m^2 \cdot K$
a_2	0	$W/m^2 \cdot K^2$
a_5	8136	$J/m^2 \cdot K$

Assuming all the heat generated in the solar collectors is transferred to the fluid in the solar collector circuit, the heat calculated in Eq. 2-2 can be equated to $\dot{Q} = \dot{m} \cdot C_p (\vartheta_{o,sc} - \vartheta_{i,sc})$ for the glycol-based brine. Then, by replacing ϑ_m with $(\vartheta_{i,sc} + \vartheta_{o,sc})/2$ and implementing $a_2=0$ in Equation 2-2, Equation 2-3 for the outgoing temperature from the solar collector can be derived.

$$\vartheta_{o,sc} = \frac{2\Delta t \dot{m} C_p \vartheta_{i,sc} + 2A_G \Delta t \eta_{0,b}(G_{b,poa} + G_{d,poa}) - A_G \Delta t a_1(\vartheta_{i,sc} - 2\vartheta_a) - A_G a_5(\vartheta_{i,sc} - 2\vartheta_{m,prev})}{2\Delta t \dot{m} C_p + A_G \Delta t a_1 + A_G a_5} \quad (\text{Eq.2-3})$$

This equation remains applicable when the solar collector circuit is not flowing (pump is off), with the only modification being $\dot{m} = 0$.

2.1.2 Adsorption chiller

Principle of operation: Sorption cooling systems, classified as heat-driven cycles, play a crucial role in energy-efficient cooling applications. These systems operate on the principles of adsorption and absorption, where the adsorbate material either accumulates on the surface of a solid adsorbent material (adsorption) or is taken up by the bulk volume of a liquid or solid adsorbate (absorption). Both processes

release heat during sorption, necessitating external heat input to reverse the process and separate the adsorbed or absorbed material.

Regarding performance assessment, thermally driven chillers are typically evaluated based on their thermal coefficient of performance (COP), representing the ratio of the heat removed to the energy input. In contrast, conventional chillers are assessed based on the ratio of the removed heat to the electricity consumed. Generally, sorption chillers tend to have a lower COP compared to conventional compression chillers due to the thermodynamic nature of these systems. For example, for an identical cooling capacity of 10 kW, the electrically driven cooling cycle (on the left of Figure 2.4) rejects 13 kW of heat (assumed COP = 3), whereas the thermally driven cooling cycle (on the right of Figure 2.4) rejects 30 kW (assumed COP = 0.5). This in itself does not cause a problem if the supplied heat for the thermally driven cooling cycle is cheap enough, but both the cost (size) of the equipment and the electrical power consumption for the auxiliary components (pumps, fans etc.) can be a challenge and have to be considered when planning and designing a system: heat rejection accounts for up to 60% of the total electrical power used in solar driven cooling system.

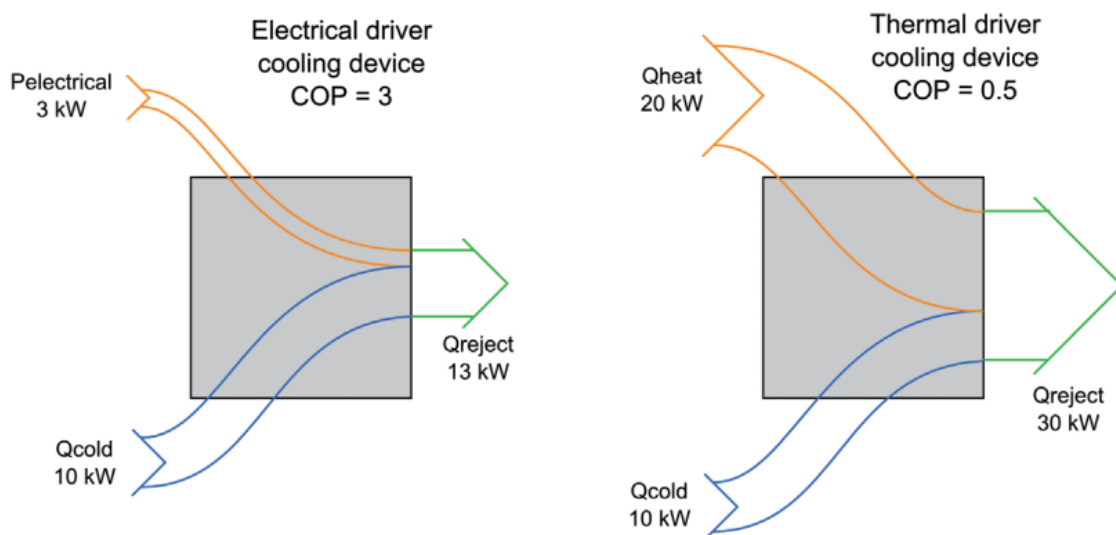


Figure 2.4 - mechanical vs. thermal cooling^[12]

Furthermore, the decision between an absorption or adsorption chiller often depends on several factors. Adsorption chillers are preferred for their ease of maintenance and extended lifespan. They perform exceptionally well in operations

requiring lower temperatures, while their effectiveness is comparable to absorption chillers in medium to high-temperature settings. Additionally, absorption chillers, similar to systems with the same cooling load and operation as SHAKK, often face limitations regarding the choice of refrigerants, thereby posing higher health and environmental risks compared to adsorption systems.

Before discussing the modeling of adsorption chiller, first the principles underlying the adsorption process will be briefly explained. Adsorption chillers employ diverse adsorption pairs, with common choices including water-silica gel and water-Zeolite. Notably, the SHAKK installation at INES utilizes the water-zeolite combination. These chillers operate within closed cycles, capable of producing chilled water with temperatures typically maintaining at a minimum of 5 to 6°C. Typically, adsorption chillers comprise two identical modules, each undergoing alternating adsorption and desorption phases. These modules function cyclically, with the system smoothly transitioning between them at regular intervals.

Figure 2.5 illustrates one complete adsorption/desorption cycle. During the adsorption phase (designated as “desorber/adsorber #2” in the compartment on the right), water, serving as the refrigerant, undergoes evaporation in the evaporator

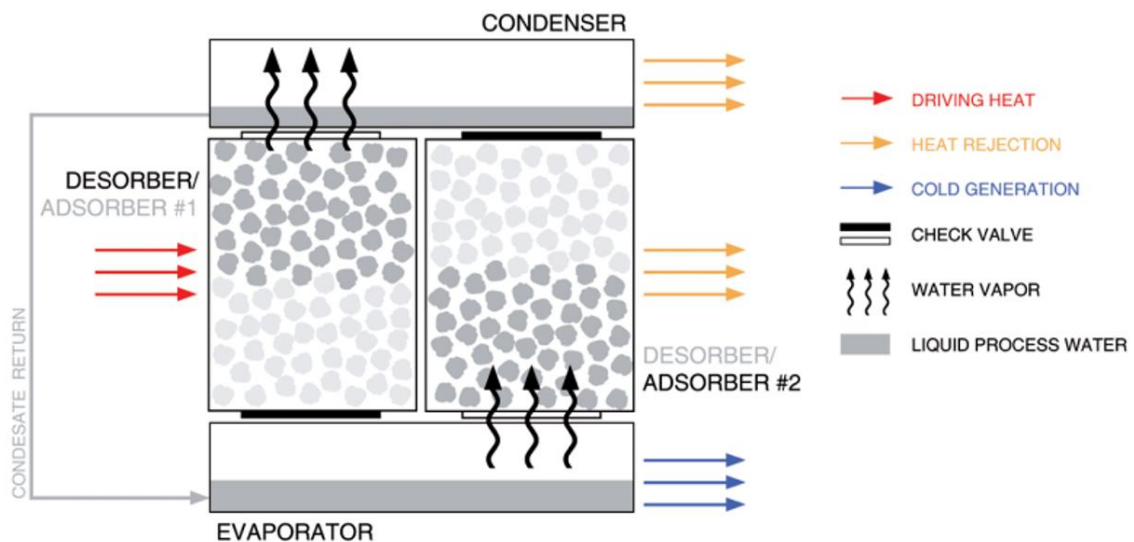


Figure 2.5 - Schematics of the operation of an adsorption chiller^[12]

and is drawn towards the adsorbent. The water vapor is then adsorbed within “desorber/adsorber #2”, specifically on the internal surface within the micro-pores of zeolite situated between the fins of a finned-tube heat exchanger. The released latent and evaporation heat from “desorber/adsorber #2” is dissipated into a cooling

water circuit, ultimately being rejected into the ambient surroundings. During the subsequent desorption phase (illustrated for “desorber/adsorber #1” in the compartment on the left), hot water flows through the heat exchanger. As the temperature rises, the adsorption capacity of the solid adsorbent decreases, leading to an increase in vapor pressure and the release of water vapor from the solid, directing it into the condenser. The same cooling water circuit utilized for the “desorber/adsorber” modules receives the latent heat during condensation. The condensed water is then returned to the evaporator for the cycle to recommence.

To run this process quasi-continuously, it is necessary to have the adsorption-desorption-modules in alternating operation mode. Figure 2.6 illustrate the distinctions between a basic adsorption cycle and a two-bed continuous adsorption cycle^[12,13].

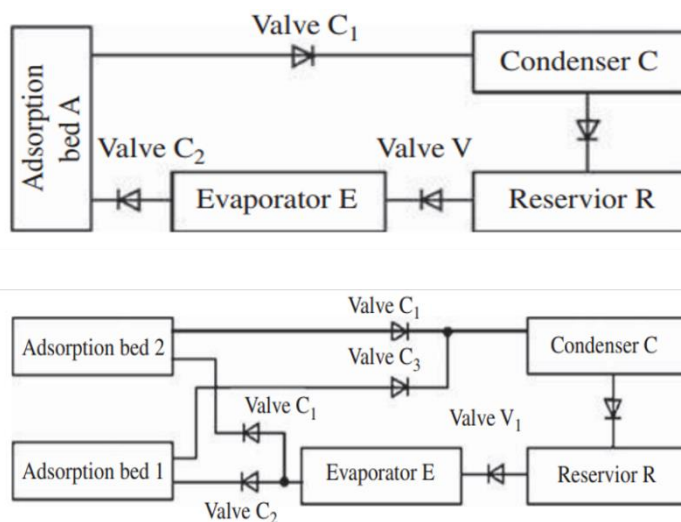


Figure 2.6 – schematics of a basic adsorption cycle (top) vs. a two-bed continuous adsorption cycle (bottom)^[13]

Principle of modeling: There are three temperature circuits flowing in the adsorption chiller, a high temperature (HT) that flows from the heat storage to help with the desorption of water from adsorbent, a intermediate temperature (MT) from the dry cooler for cooling the system, and a low temperature (LT) which is the output of the adsorption chiller and will charge the cold storage.

In modeling of adsorption chiller, an empirical model developed by the manufacturer was used that can indicate the $\dot{Q}_{cooling}$ and $COP_{thermal}$ of the adsorption unit based on the inflowing temperatures of the three temperature circuits. It can be generally represented as:

$$\text{quantity} = a + b \cdot H + c \cdot S + d \cdot H^2 + e \cdot S^2 + f \cdot H \cdot S \quad (\text{Eq.2-4})$$

Where $H = MT - LT$ and $S = HT - MT$ and the regression coefficients a to f vary depending on whether they are utilized to calculate the \dot{Q}_{cooling} or the $\text{COP}_{\text{thermal}}$.

Figure 2.7 shows the energy flow of the adsorption chiller. \dot{Q}_{heating} is the energy that drives the system and is received from energy stored in the heat storage, \dot{Q}_{cooling} is taken from the cold fluid flowing from the cold storage, and \dot{Q}_{reject} is the energy that was provided by the dry cooler for cooling purposes.

For a thermally driven cooling system, the $\text{COP}_{\text{thermal}}$, which indicates the required heat input for the cold production, varies with the equipment operation conditions, i.e., the three temperature levels. It can be stated as the ratio of the desired output \dot{Q}_{cooling} to the driving force \dot{Q}_{heating} . By knowing the \dot{Q}_{cooling} , $\text{COP}_{\text{thermal}}$ and the inflow temperatures of each level, the outflow temperatures can be calculated.

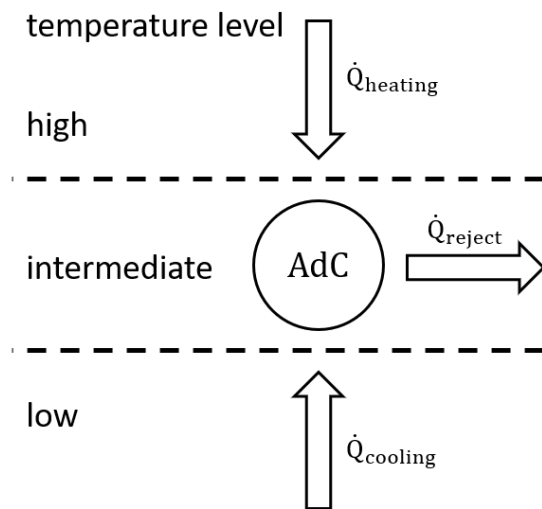


Figure 2.7 - Energy flow of adsorption chiller

2.1.3 Reversible heat pump

Fahrenheit GmbH^[8] has incorporated a Glycol-base brine-water reversible heat pump with Propane as the refrigerant into the SHAKK system. This machine serves as a compression chiller when the requirements for adsorption chiller operation are not met. It also functions as a heat pump to fulfill heat demands during the cold season.

Since only the inflow temperatures of the source and sink sides are known at each timestep, the decision was made to develop 2-dimensional 2nd-order polynomial regression model. This model predicts the electrical power consumption P_{elec} , the cooling capacity $Q_{cooling}$ when operating as the compression chiller or the heating capacity $Q_{heating}$ when operating as the heat pump, based on the fluids flowing in the condenser and evaporator, assuming 5K temperature difference between the refrigerant and the heat transfer fluid (HTF). The training data for the regression models and operation limitation for the temperatures are obtained from the manufacturer's datasheet and can be found in the appendix. In both cases, it is assumed that in each iteration, the temperature in the condenser increases by 5K based on the work done by Sawant.P^[14].

Compression chiller

Principle of operation: When the reversible heat pump (RHP) operates as a chiller, the condenser is connected to the outdoor coil heat exchanger, and water flows on this side. The evaporator side of the chiller, containing brine, is connected to the low-temperature storage unit heat exchanger. Figure 2.8 illustrates this setting.

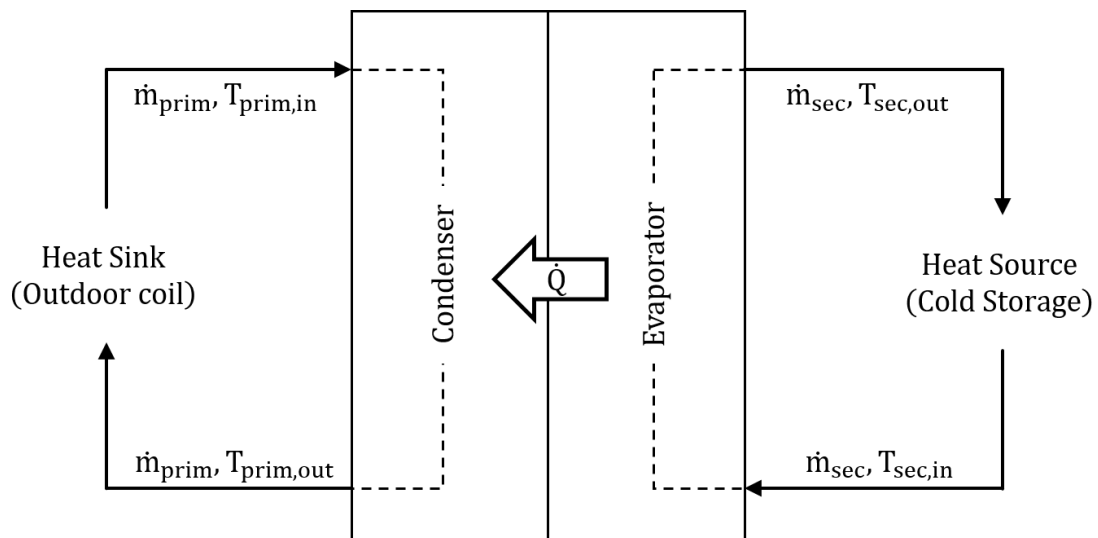


Figure 2.8 - Energy flow in the compression chiller

Principle of modeling: The 2nd-order polynomial regression model accurately predicts the cooling capacity and power consumption of the chiller for various combinations of evaporator and condenser temperatures. The model, expressed as Eq.2-5, has been trained with data obtained from the manufacturer's datasheet, and the respective regression coefficients are presented in Table 2.2.

$$\text{quantity} = a + b \cdot T_{\text{cond}}^2 + c \cdot T_{\text{cond}} + d \cdot T_{\text{cond}} \cdot T_{\text{evap}} + e \cdot T_{\text{evap}} + f \cdot T_{\text{evap}}^2 \quad (\text{Eq.2-5})$$

After training, the outgoing temperature of the fluids from the condenser can be calculated.

Table 2.2 - regression coefficients of the compression chiller model

coefficients	a	b	c	d	e	f
Q_{cooling} [kW]	46.19	- 0.238	1.497	- 0.002	- 0.008	0
P_{elec} [kW]	2.379	0.192	- 0.076	- 0.001	0.004	- 0.001

Heat pump

Principle of operation: In the heat pump operation, brine flows from the heat source (solar collector or outdoor coil depending on the operation condition) into the evaporator, while water from the hot storage flows in the condenser. The input and output values of the heat pump can be seen in Figure 2.9.

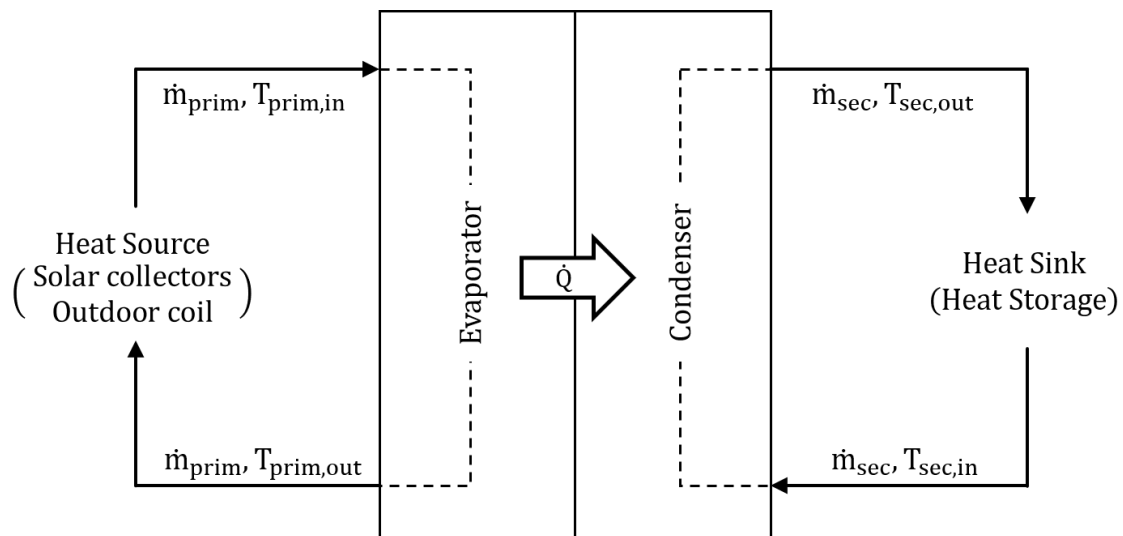


Figure 2.9 - Energy flow in the heat pump

Principle of modeling: Similar to the compression chiller model, the same polynomial model regression model (Eq. 2-5) is employed for the heat pump. However, distinct coefficients are utilized for this mode, where the source is connected to the evaporator, and the sink is connected to the condenser. The calculated coefficients are shown in Table 2.3.

Table 2.3 - regression coefficients of the heat pump model

coefficients	a	b	c	d	e	f
Q_{heating} [kW]	34.255	- 0.440	0.983	- 0.001	- 0.003	0.007
P_{elec} [kW]	1.707	0.132	- 0.054	0	0.003	- 0.001

2.1.4 Dry cooler / Outdoor coil

Principle of operation: Dry coolers typically consist of finned heat exchangers (air to water), fans, and a casing. Water circulates in a closed circuit, and by passing ambient air over the finned surfaces, heat is rejected to the air (Figure 2.10). The outdoor coil primarily functions as a dry-cooling tower. It serves as the heat-sink for the condenser of the chillers and the heat-source for the evaporator of the heat pump [12].

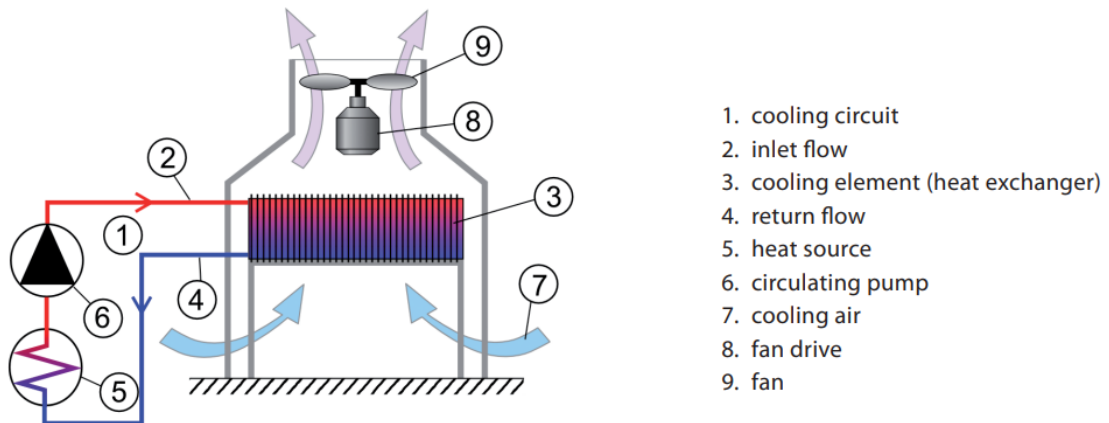


Figure 2.10 - Sketch of a dry cooler [12]

Principle of modeling: Assuming the outdoor coil functions as a cross-flow air-fluid heat exchanger, with homogeneous air flow, no pressure loss, and a constant overall heat transfer coefficient, its model is derived from the effectiveness-NTU method (Number of Transfer Units). This method determines actual transferred heat value using the effectiveness (ϵ) of a heat exchanger and the maximum possible heat transfer achievable hypothetically. The process is summarized by the following equations [14]:

$$\dot{Q}_{\text{real}} = \epsilon \cdot \dot{Q}_{\text{max}} \quad (\text{Eq.2-6})$$

$$\epsilon = 1 - \exp\left(\frac{NTU^{0.22}}{c} \cdot (\exp(-c \cdot NTU^{0.78}) - 1)\right) \quad (\text{Eq.2-7})$$

$$\dot{Q}_{\max} = C_{\min} (T_{h,in} - T_{c,in}) \quad (\text{Eq.2-8})$$

$$NTU = \frac{U \cdot A_s}{C_{\min}} \quad (\text{Eq.2-9})$$

$$c = \frac{C_{\min}}{C_{\max}} \quad (\text{Eq.2-10})$$

Here, c represents the capacity ratio, C_{\min} and C_{\max} denote the smaller and larger of the heat capacity rates of the hot and cold sides ($C = \dot{m} \cdot c_p$), U is the overall heat transfer coefficient, A_s is the heat transfer surface area, and NTU is the unitless number of transfer units. Table 2.4 provides the parameters of the outdoor coil utilized in the SHAKK system.

Table 2.4 - Outdoor coil parameters

Parameter	Value	Unit
U	31.2	$W/m^2 \cdot K$
A_s	561.5	m^2

2.1.5 Thermal storages

Principle of operation: In cooling systems, a cold storage component can be incorporated. This integration facilitates the operation of the chiller during non-peak hours, thus enhancing its efficiency in conventional cooling systems, storage has become one of the primary solutions to overcome the electric power imbalance between daytime demand and nighttime availability. The storage unit uses off-peak power to provide cooling capacity by extracting heat from a storage medium. Typically, a storage system uses refrigeration equipment at night to operate more efficiently than during the day, reducing the power consumption, and to create a reservoir of cold material. During the day, the reservoir is tapped to provide cooling power.

In a solar-assisted system, the reason to install a storage unit is somewhat different. The primary objective is to maximize the utilization of solar energy to address periods of reduced radiation, during which solar heat alone may not suffice to meet the cooling demands. This objective is achieved by generating surplus cooling power during periods of ample solar gains. In this regard, it is of importance to

acknowledge the differences that often arise between solar gains and cooling demands on a daily basis. These differences originate from typical load patterns, where peak cooling requirements typically appear in the afternoon or evening, while solar gains tend to reach their highest point around noon. In such cases, the storage system must be engineered to accommodate the cooling demand over several hours.

SHAKK system employs two thermal storage units; one unit stores hot water for supplying the adsorption chiller during cooling operations or simply stores hot water during heating modes, while the other unit stores cold water for use during cooling operations. For the modeling it is assumed that both storages are of equal size and dimensions, and well-insulated. Table 2.5 provides the parameters of these storage units. The Heat storage is used in both cooling and heating modes. During the cooling mode, it connects with the collector array through a heat exchanger, simultaneously establishing a direct link to the high-temperature circuit (HT circuit) of the adsorption chiller. Conversely, in the heating mode, it exclusively connects directly to the condenser of the heat pump. In contrast, the cold storage is solely utilized during the cooling operation. It either directly connects to the low-temperature circuit (LT circuit) of the adsorption chiller or links to the evaporator of the compression chiller via a heat exchanger.

Table 2.5 - Thermal storage parameters

Parameter	Symbol	Value	Unit
Height	H	2.05	m
Outer diameter	D	0.79	m
Thickness	D _{th}	0.02	m
Heat transfer coef.	k	0.00 ¹	W/m ² .K

The performance of the system is largely evaluated based on how quickly it can reach and maintain desired temperatures in these thermal storage units. Both thermal storages feature connection points located at the top and bottom. The volume flow rate and flow direction vary according to the type of storage and the

¹ The value for the heat transfer coefficient has been assumed to be negligible due to the insulation. However, the parameter is included in the model, allowing for future necessary adjustments.

operation mode. In the absence of a real load profile, for better comparison between operation in the similar modes with different components, a constant load has been assumed in the shape of a constant discharge from the end-of-the-line thermal storage and returning at a constant temperature.

Principle of modeling: The modeling of the thermal storages was based on the stratified model proposed by Sawant.P [15], in which the thermal storage unit was conceptualized as a layered cylindrical structure. In this model, the temperature at each layer is determined through an energy balance analysis, making the mass at each layer and the entering or exiting volume flow at the control volume crucial parameters. Figure 2.11 depicts the configurations of the storage units for better comprehension.

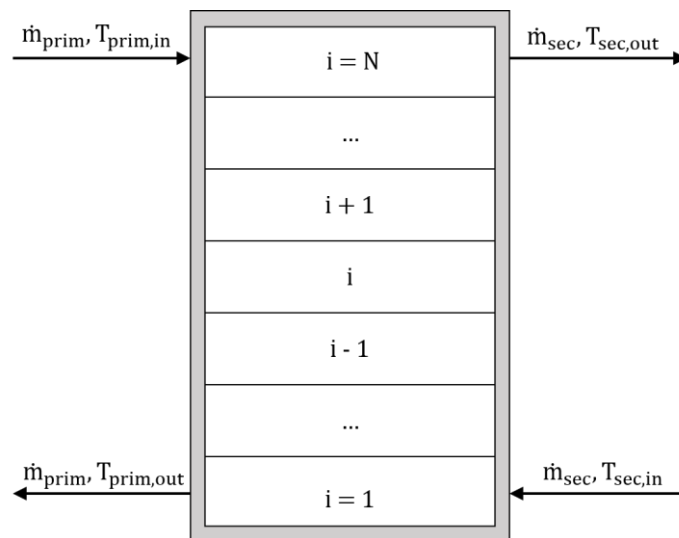


Figure 2.11 - Schematics of the thermal storage unit

The model relies on the Fourier equation to calculate the change in internal energy of each layer. It accounts for four heat transfer mechanisms: **mass transport into the storage** in the top and bottom layers, **mass transport within the storage** due to identical effective mass transport, **heat loss to the environment** at all layers, and **conduction** between neighboring layers. These mechanisms are expressed as differential equations provided in Table 2.6 for respective top, middle, and bottom layers, along with their corresponding flow directions (positive or negative mass flow rate values). A positive mass flow rate indicates a flow from top to bottom, while a negative mass flow value signifies the opposite direction. Table 2.7 provides

additional explanations about the parameters utilized in Table 2.6 and their corresponding equations.

Table 2.6 - governing equations in thermal storage units

Layer	\dot{m}	Equation	Eq. no
Top	+	$m_N C_p \frac{dT_N}{dt} = \dot{m}_{prim} C_p (T_{prim,in} - T_{N,prev}) - k A_{ext} (T_{N,prev} - T_{amb}) + \frac{A_i \cdot \lambda_{eff}}{z_i} (T_{N-1} - T_N)$	2-11
	-	$m_N C_p \frac{dT_N}{dt} = \dot{m}_{prim} C_p (T_{prim,in} - T_{N,prev}) - k A_{ext} + \dot{m}_i C_p (T_{N,prev} - T_{N-1}) + \frac{A_i \cdot \lambda_{eff}}{z_i} (T_{N-1} - T_N)$	2-12
Middle	+	$m_i C_p \frac{dT_i}{dt} = -k A_{ext} (T_{i,prev} - T_{amb}) + \dot{m}_i C_p (T_{i+1} - T_{i,prev}) + \frac{A_i \cdot \lambda_{eff}}{z_i} (T_{i+1} - 2T_{i,prev} + T_{i-1})$	2.13
	-	$m_i C_p \frac{dT_i}{dt} = -k A_{ext} (T_{i,prev} - T_{amb}) + \dot{m}_i C_p (T_{i,prev} - T_{i-1}) + \frac{A_i \cdot \lambda_{eff}}{z_i} (T_{i+1} - 2T_{i,prev} + T_{i-1})$	2.14
Bottom	+	$m_1 C_p \frac{dT_1}{dt} = -\dot{m}_{sec} C_p (T_{1,prev} - T_{sec,in}) - k A_{ext} (T_{1,prev} - T_{amb}) + \dot{m}_i C_p (T_{1+1} - T_{1,prev}) + \frac{A_i \cdot \lambda_{eff}}{z_i} (T_{1+1} - T_{1,prev})$	2-15
	-	$m_1 C_p \frac{dT_1}{dt} = -\dot{m}_{sec} C_p (T_{1,prev} - T_{sec,in}) - k A_{ext} (T_{1,prev} - T_{amb}) + \frac{A_i \cdot \lambda_{eff}}{z_i} (T_{1+1} - T_{1,prev})$	2-16

Table 2.7 - Parameters and Equations for Thermal Storage Modeling

Parameter	Description	equation
z_i	height of the layer	$\frac{H}{N}$
A_{ext}	external area of the layer	$\pi \cdot D \cdot z_i$
A_i	cross-sectional area of the layer	$\frac{\pi(D - 2D_{th})^2}{4}$
m_i	mass of water in the layer	$A_i \cdot z_i \cdot \rho$
\dot{m}_i	mass flow rate in the layer	$\dot{m}_{prim} - \dot{m}_{sec}$

In modeling of the thermal storages, the number of layers has been decided to be set at 4 for heat storage and 3 for cold storage, due to their relatively high-volume

flow rate and the error it would occur due to the complete change of the simulation volume before reaching the next timestep.

2.1.6 Heat Exchangers

Principle of operation: Heat exchangers are vital components in various engineering systems designed for efficient heat transfer between two or more fluids. At their core, heat exchangers facilitate the transfer of thermal energy from one fluid to another, without the fluids coming into direct contact with each other. This thermal exchange can involve heating, cooling, or both, depending on the specific requirements of the system^[15].

Principle of modeling: In the SHAKK system, three heat exchangers have been employed, all of which are of the counter-flow type. While the effectiveness-NTU method, discussed in Chapter 2.1.4, remains applicable for modeling, the equation for calculating effectiveness differs due to the counter-flow configuration of the heat exchangers. For counter-flow heat exchangers, the effectiveness was calculated using the following equation:

$$\varepsilon = \frac{1 - \exp(-NTU \cdot (1 - c))}{1 - c \cdot \exp(-NTU \cdot (1 - c))} \quad (\text{Eq.2-17})$$

This equation accounts for the specific characteristics of counter-flow heat exchangers. The rest of the equations discussed previously (2-6, 2-8, 2-9, and 2-10) remain applicable for modeling the heat exchangers. Table 2.8 provides the parameters of each heat exchanger and their placement in the system.

Table 2.8 - Parameters of the heat exchangers

No.	Primary side	Secondary side	A [m ²]	U [kW/m ² ·k]
1	solar collector	heat storage	10.0	2.20
2	outdoor coil	chillers	15.6	2.29
3	compression chiller	cold storage	7.66	2.20

2.2 Modeling of the Operation modes

The SHAKK system comprises a solar collector array from AKOTECH GmbH^[7], Hybrid container housing an Adsorption chiller and Reversible heat pump, a dry cooling tower, and two thermal storage units for hot and cold applications, all sourced from Fahrenheit GmbH^[8].

This versatile system has the capability to supply both heat and cold, adapting to varying demands and seasonal conditions. Further discussed in detail on this functionality will be provided in detail in the upcoming chapter.

2.2.1 Cooling modes

During cooling operations, the system's performance is influenced by the ambient temperature and irradiance levels, allowing it to smoothly shift between two specific cooling methods: via the adsorption chiller or via the compression chiller. The subsequent section will offer a thorough explanation of each cooling approach, clarifying their distinct functions and illustrating how the system adeptly adjusts to the current environmental conditions.

Cooling via adsorption chiller

This operational mode becomes active under conditions of moderate to high solar irradiance and warm ambient air temperature. Within this mode, the collector array raises the brine temperature, directing the accumulated heat to the high-temperature storage. Subsequently, the heat flows into the adsorption chiller upon reaching the designated operational temperature limit. Within the adsorption chiller, three circuits operate concurrently. The high-temperature (HT) circuit maintains temperatures between 70-90°C, the intermediate-temperature (MT) circuit ranges between 25 and 45°C, and the low-temperature (LT) circuit spans from 20 to 10°C. The MT circuit connects to a heat exchanger leading to the cooler, while the LT circuit is directly linked to the low-temperature storage. The adsorption chiller, in turn, contributes to cooling the cold storage. Figure 2.12 illustrates the system diagram during this operation mode.

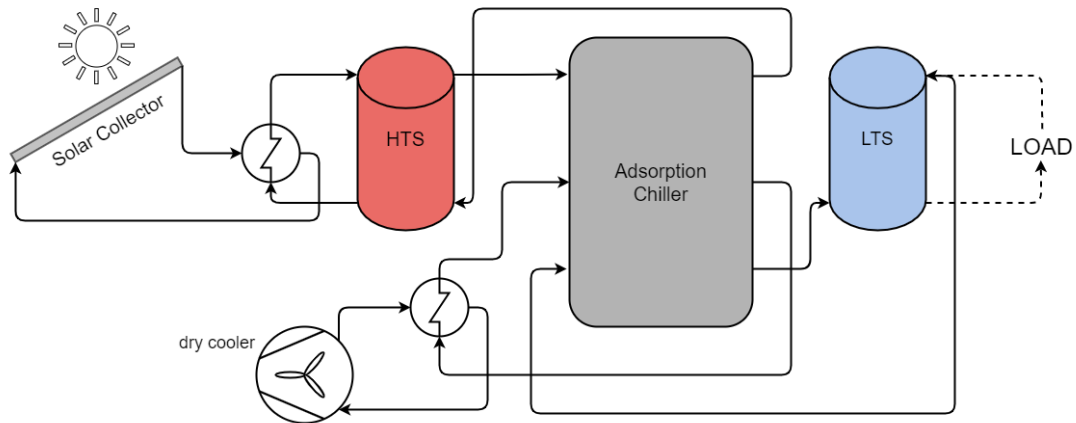


Figure 2.12 - schematics of the system under cooling via adsorption chiller mode

Cooling via compression chiller

This operational mode is initiated when solar irradiance is insufficient to elevate the temperature within the high-temperature storage to 90°C. In such instances, the solar collectors continue to warm the hot storage, but this heat is not utilized by the adsorption chiller. Instead, the cooler functions as an outdoor coil, directing heat to a heat exchanger and then to the compression chiller. The compression chiller further utilizes a heat exchanger system, cooling the chilled brine before directing it to the cold storage. The entire system diagram during this operation mode is depicted in Figure 2.13.

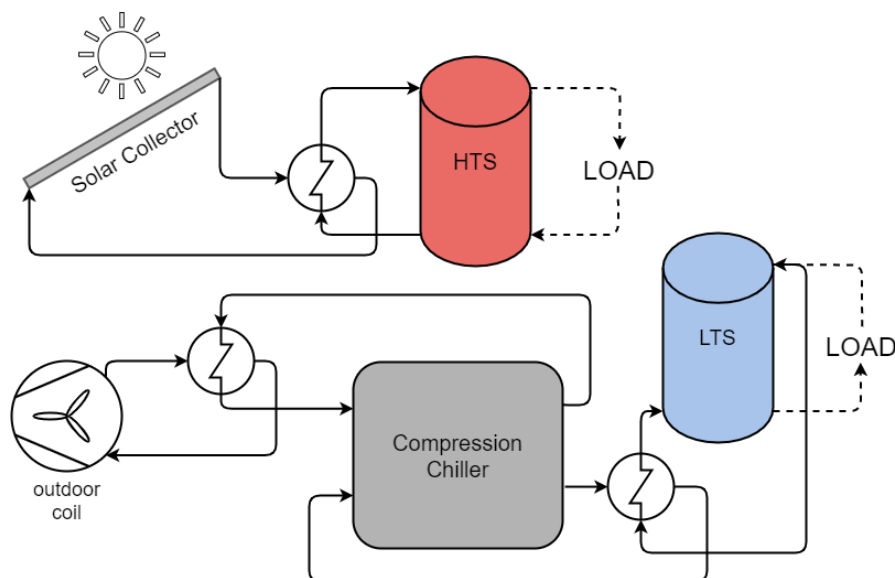


Figure 2.13 - schematics of the system under cooling via compression chiller mode

2.2.2 Heating modes

While the primary purpose of the system is to provide cooling, it also possesses the capability to generate heat during colder seasons. To achieve this, the system incorporates a heat pump, with either the solar collector or the outdoor coil serving as its heat source. It is important to note that utilizing outdoor coil could lead to increased electrical consumption due to the relatively higher energy consumption of the outdoor coil compared to the collector array. Therefore, balancing the benefits of a steadier temperature inflow against potential higher energy consumption becomes a crucial consideration in optimizing system performance in the heating operation modes. The following sections will elaborate on each of these components in greater detail.

Heating via solar collectors

When solar irradiance is sufficiently high, the system incorporates solar collectors for heating purposes. Once the temperature within the solar collector reaches the specified operational limits, indicating favorable conditions, the pump activates to circulate brine directly to the heat pump. Concurrently, the water within the hot storage unit experiences warming. This process ensures efficient utilization of solar energy for heating, providing an eco-friendly and sustainable heating solution. Figure 2.14 captures the flow in this operation mode.

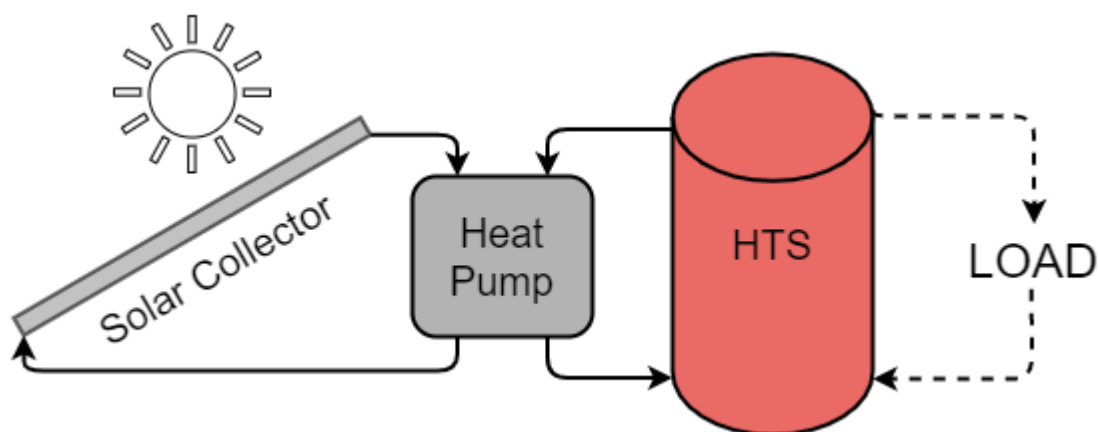


Figure 2.14 - schematics of the system under heating via solar collectors' mode

Heating via outdoor coil

As it is illustrated in Figure 2.15, this heating operation follows a similar process to that employed with solar collectors, with the key difference being that the outdoor coil acts as the heat source for the heat pump instead of the collector array. This

distinction may result in a more consistent temperature inflow for the heat pump, thereby enhancing operational stability.

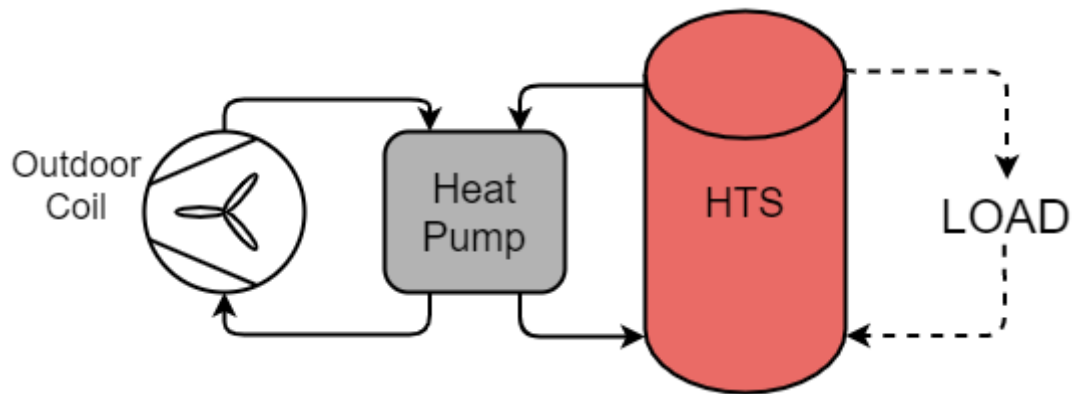


Figure 2.15 - schematics of the system under heating via outdoor coil mode

3 Simulation and results

In the previous chapter, the fundamental principles underlying the modeling complexities of each component within the SHAKK system were explored. A sturdy theoretical foundation was established, setting the stage for the practical exploration undertaken in this chapter. Here, each operational mode within the system was simulated, with a focus on examining the dynamics of various scenarios or specific days. Comprehensive analysis and discussion were conducted, with each mode being carefully examined. Through this process, the intricacies of system behavior under differing circumstances were revealed, providing insights into its operational efficacy and potential areas for optimization. This chapter served as a crucial bridge between theoretical understanding and practical application, paving the way for a deeper comprehension of the real-world performance of the SHAKK system.

The dataset utilized in the simulation primarily consists of weather data collected from the Weather Station located at the INES building, comprising the ambient temperature and global irradiance on the horizontal plane. For this study, data from the winter of 2021 and the summer of 2022 were employed.

Originally, the simulation employed a step size of 15 minutes, a standard value in energy technology consistent with the dataset's original time resolution. However, due to high volume flow rates in specific system components, such as the cold storage unit, the step size was refined to 1 minute to enable more accurate simulation. Consequently, the dataset was subjected to interpolation to align with the adjusted time increments. It is assumed that all state variables remain constant within a time step, indicating steady-state operation.

Furthermore, certain models require direct and diffuse radiation inputs. To address this requirement, the Boland-Ridley-Lauret model^[17] was utilized to convert global radiation into diffuse and direct components. The subsequent equations (Eq.3-1) depict the relationship utilized, with a nominal value of 1367 W/m^2 representing extraterrestrial radiation, where G represents the instance's global irradiance value in W/m^2 . Following this, using the PV-lib^[6] library in Python, the values of direct and diffuse irradiances for the plane of array were determined, enabling their application to solar collectors, as discussed in Chapter 2.1.1.

$$I_{dif} = \frac{1}{1 + \exp\left(7.997\left(\frac{G}{1367} - 0.586\right)\right)} \cdot G \quad (\text{Eq.3-1})$$

$$I_{dir} = G - I_{dif}$$

3.1 Cooling via adsorption chiller

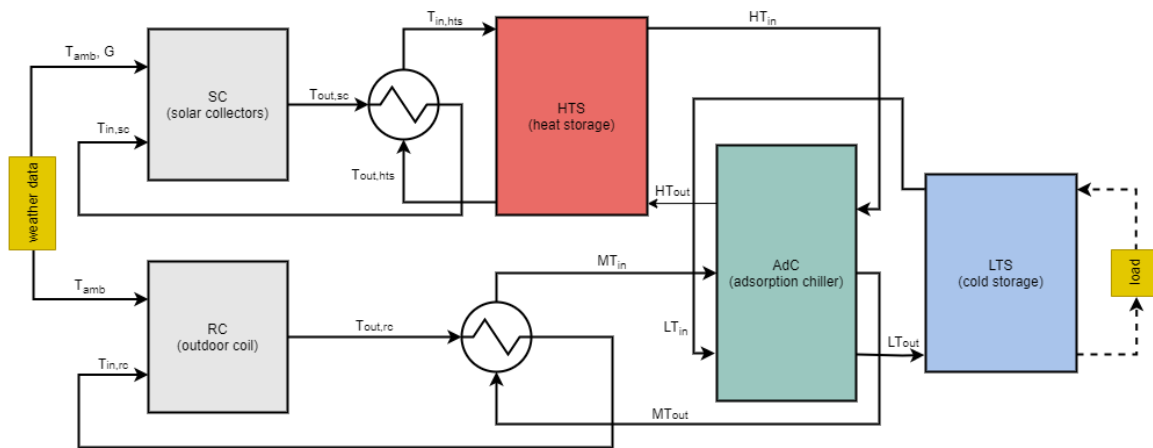


Figure 3.1 - Schematics of the data flow in cooling via the adsorption chiller operation mode

In the cooling operation modes, the objective is to reduce the temperature within the cold storage to a target of 10°C. Operating the SHAKK system in cooling mode through the adsorption chiller necessitates a high temperature range for the desorption phase. Consequently, a sunny day presents the optimal conditions for efficient operation. For the simulation, the date chosen was June 10, 2022. This particular day had the highest average irradiance, with direct irradiance peaking above 700 W/m², and total irradiance reaching above 1000 W/m². Moreover, the ambient temperature exhibited a consistent range throughout the day, fluctuating between 10.80°C and 25.35°C (Figure 3.2).

Table 3.1 - volume flow rates values in between components

from	to	Volume flow rate [m ³ /h]
Solar collectors	HT heat exchanger	1.40
HT heat exchanger	Heat storage	1.36
Heat storage	Adsorption chiller	3.00
Outdoor coil	MT heat exchanger	9.38
MT heat exchanger	Adsorption chiller	6.30
Adsorption chiller	Cold storage	12.0

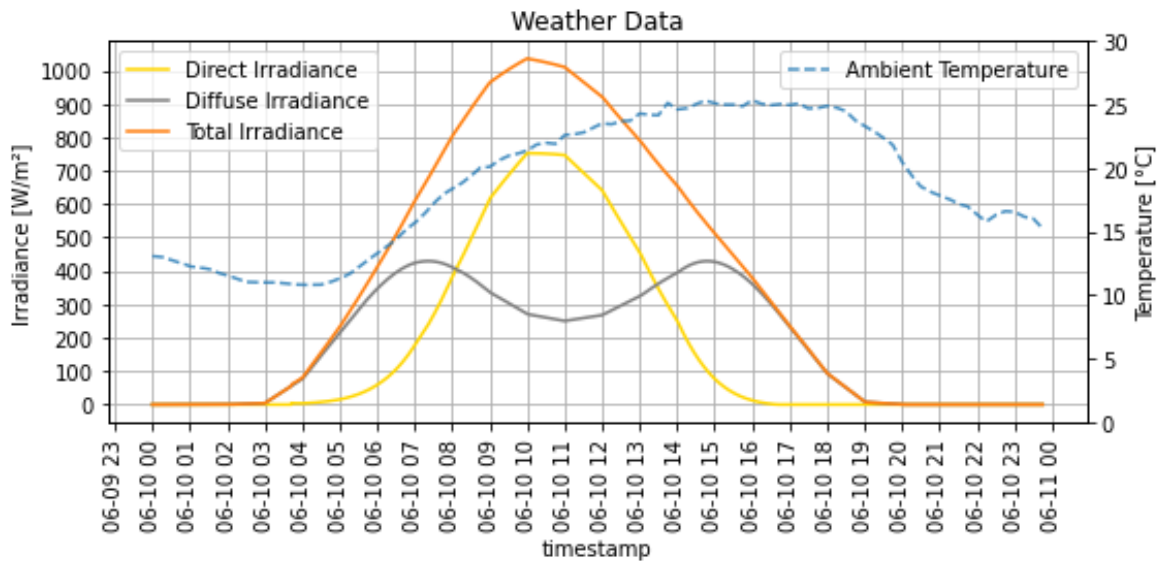


Figure 3.2 – Irradiance and temperature changes during the day 10.6.2022

At the beginning of the simulation, the temperatures at the solar collectors, heat storage, outdoor coil, and adsorption chiller are assumed to be equal to the ambient temperature. The volume flow rates in different circuits of the system are detailed in Table 3.1. Additionally, a constant load flow of 1 m³/h and 20°C was assumed in the low temperature storage for a more realistic simulation in the absence of actual load profile.

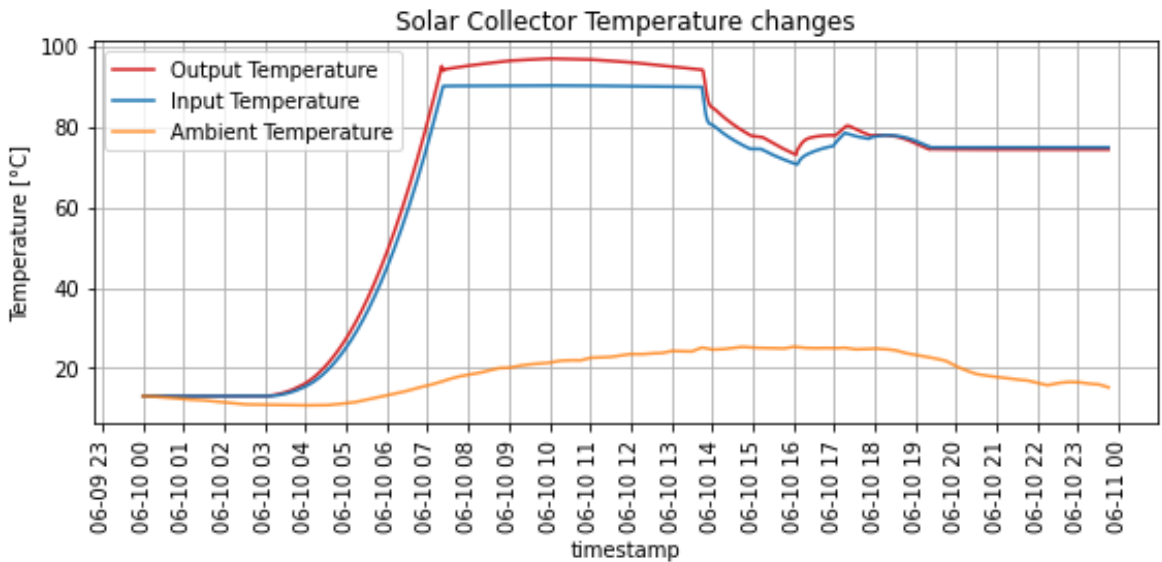


Figure 3.3 - Temperature changes in the solar collectors

The employed regression model for the adsorption chiller is valid for temperatures ranging between 70°C and 90°C in the high-temperature circuit, 25°C and 45°C for the intermediate-temperature circuit, and 10°C and 20°C for the low-temperature

circuit. Consequently, these ranges have been established as the operational limits of the adsorption chiller. Figure 3.4 illustrates the temperature changes in the mentioned circuits, along with the operational status of the solar collectors array, adsorption chiller, and outdoor coil.

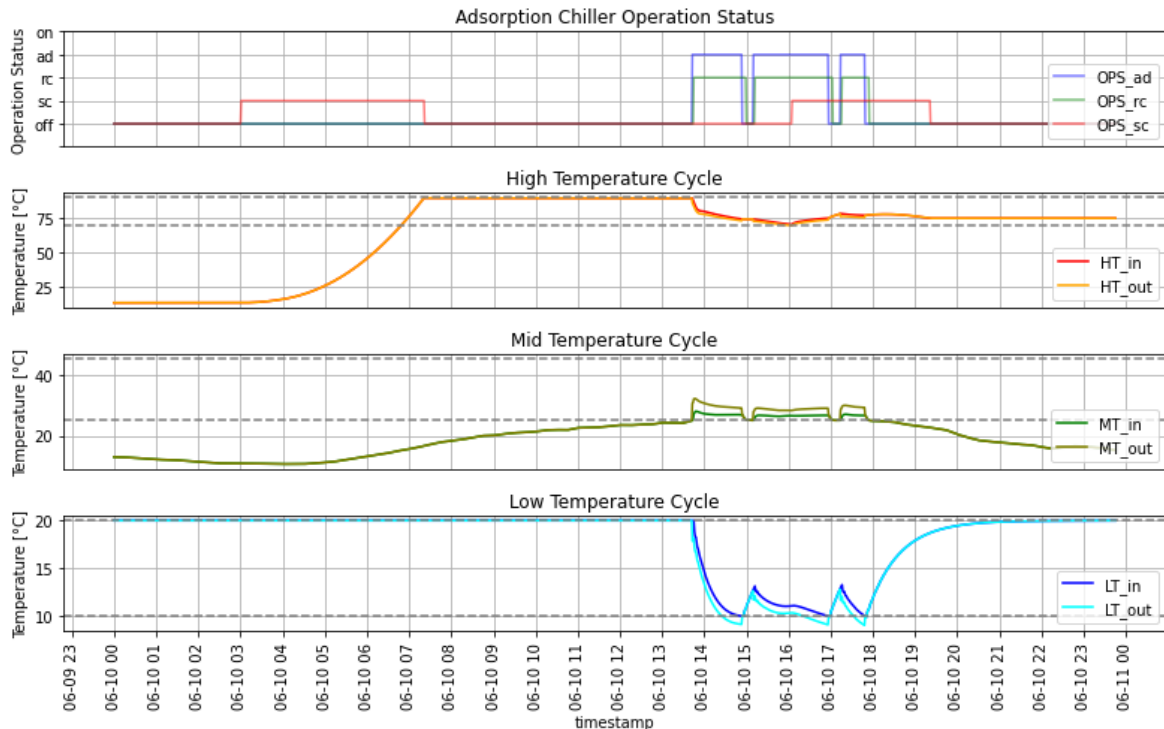


Figure 3.4 - Adsorption chiller's temperature changes

The high temperature (HT) fluid flows directly from the heat storage, meaning when the solar collectors heat up the water in the storage unit above 70°C, the operation limit in the adsorption chiller for the high temperature circuit is met. However, the solar collector circuit halts circulation when the temperature in the heat storage reaches 90°C, which is the maximum allowable temperature for the adsorption chiller in the simulation.

The low temperature (LT) circuit is connected to the low temperature storage on the other end. Due to the load assumptions explained earlier, the temperature remains at 20°C until the adsorption chiller initiates operation. To that mean, When the MT circuit temperature surpasses 25°C, the adsorption chiller begins working for the first time, extracting heat from the water flowing in the LT circuit. Consequently, the temperature in the low temperature storage (LTS) decreases until it reaches the set temperature 10°C in the LTS and the adsorption chiller. Meanwhile, the solar collector resumes operation as soon as the temperature in the high temperature

storage (HTS) falls below 70°C due to the chiller's operation. The machine starts operating again when the load increases the temperature in the LTS up to 13°C. This cyclic behavior continues as long as the operational conditions are met. In this scenario, the system stops again when the intermediate temperature MT falls below the 25°C threshold.

The performance evaluation of adsorption chillers typically involves assessing the thermal coefficient of performance ($COP_{thermal}$), which represents the ratio of heat removed to the driving heat of the chiller. In the case of a typical adsorption chiller, the $COP_{thermal}$ typically ranges from 0.2 to 0.6^[18].

Figure 3.5 provides a graphical representation of the changes in $COP_{thermal}$ at each timestep, alongside the cooling and heating capacities. Throughout the simulation, the COP value consistently fell within the range of 0.28 to 0.41. As a result, the average $COP_{thermal}$ value was calculated to be 0.35.

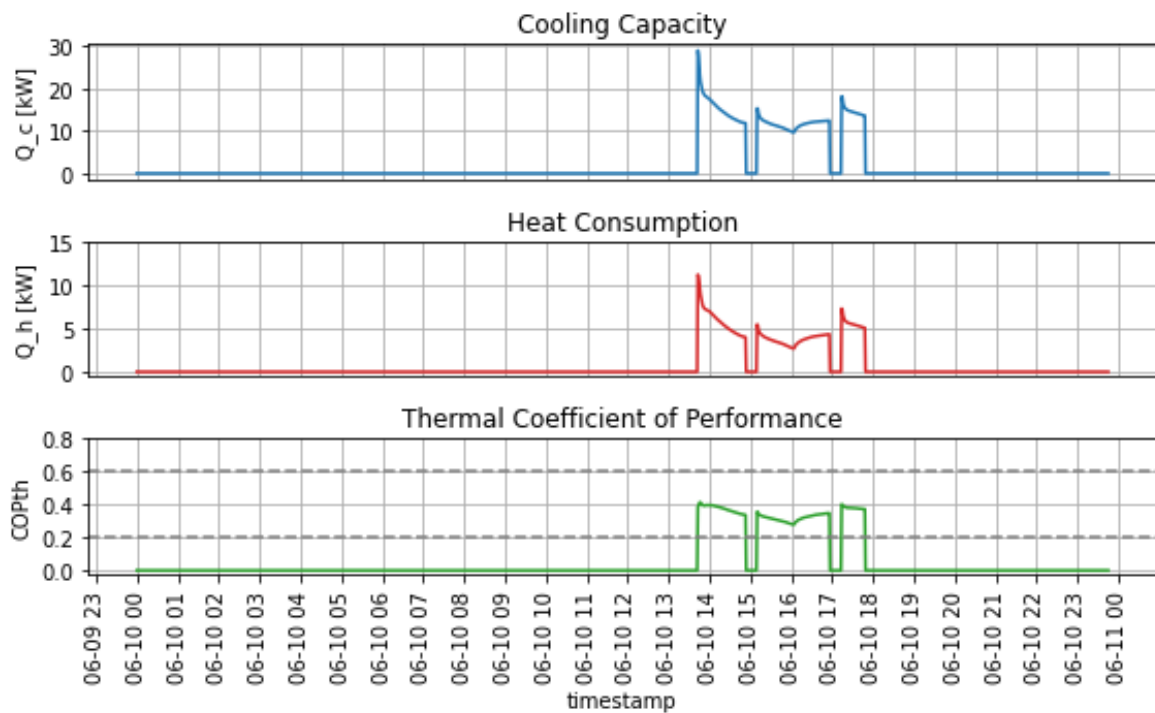


Figure 3.5 - Adsorption Chiller's COP changes

3.2 Cooling via compression chiller + Heating via solar collectors

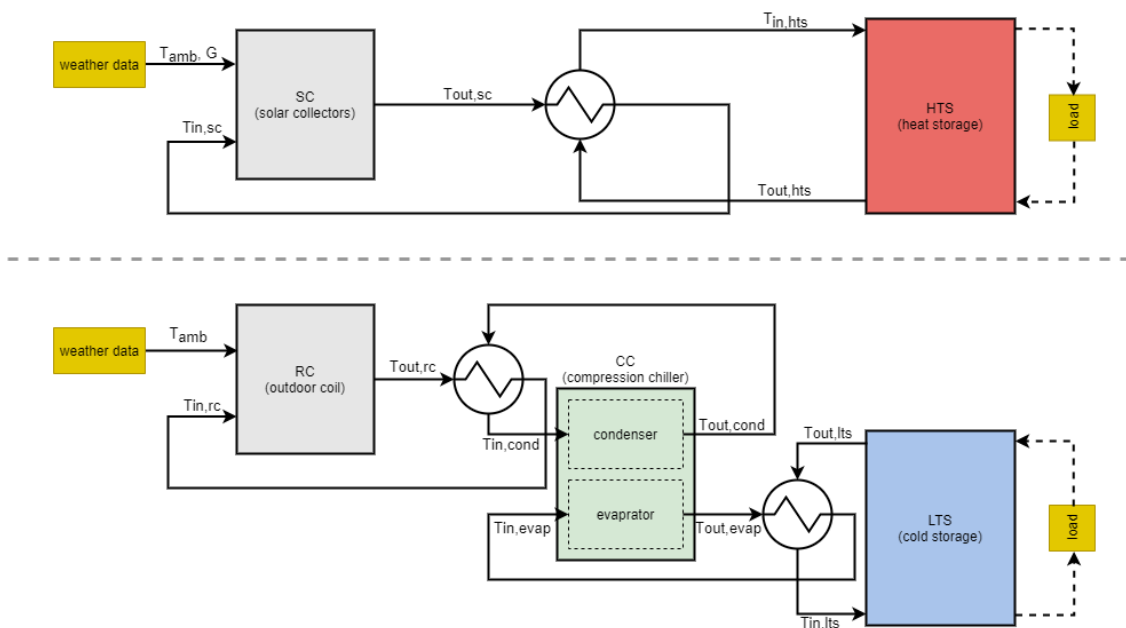


Figure 3.6 - Schematics of the data flow in cooling via the compression chiller operation mode

The need for utilizing the compression chiller arises when solar irradiance levels aren't adequate to operate the adsorption chiller effectively. In this simulation mode, the outdoor coil acts as the heat sink for the compression chiller, aiding in cooling the low-temperature storage unit. While the solar collectors and heat storage remain active, their functions are separate from other components. Figure 3.6 illustrates the operation of these two circuits and the flow of data within them.

For the sake of comparison, the similar simulation date (June 10, 2022) as the previous chapter 3.1 was maintained, along with the same initial conditions and load parameters. However, there are differences in volume flow rates, as detailed in Table 3.2. Additionally, a constant load flow was assumed for the high-temperature storage to enable scrutiny of both the heating and cooling circuits, flowing at a rate of 1 m³/h with a temperature of 20°C. Figure 3.7 shows the temperature variations of the heat transfer fluid in the solar collector circuit. Similar to the previous mode, the pump stops when the temperature in the HTS exceeds 90°C and resumes when it falls below 70°C. Given the high irradiance levels on the chosen simulation date illustrated in Figure 3.2, the system easily reaches the maximum temperature and maintains it within the specified range until irradiance is not enough, gradually

lowering the thermal storage temperature to match the constant load flow temperature.

Table 3.2 – volume flow rates values in between components

from	to	Volume flow rate [m ³ /h]
Heating circuit		
Solar collectors	HT heat exchanger	1.40
HT heat exchanger	Heat storage	1.36
Cooling circuit		
Outdoor coil	MT heat exchanger	9.38
MT heat exchanger	Compression chiller	6.30
Compression chiller	LT heat exchanger	6.00
LT heat exchanger	Cold storage	12.0

However, within cooling cycle, as shown in Figure 3.8, the system remains inactive for most of the day, with the low-temperature storage temperature maintained at the constant load flow temperature. Once the compression chiller's operational temperature criteria are met, the system cools the water in the storage tank to the target temperature of 10°C. Afterward, it shuts off until the temperature increases above 13°C, repeating this cycle until the operational temperature requirements are no longer met.

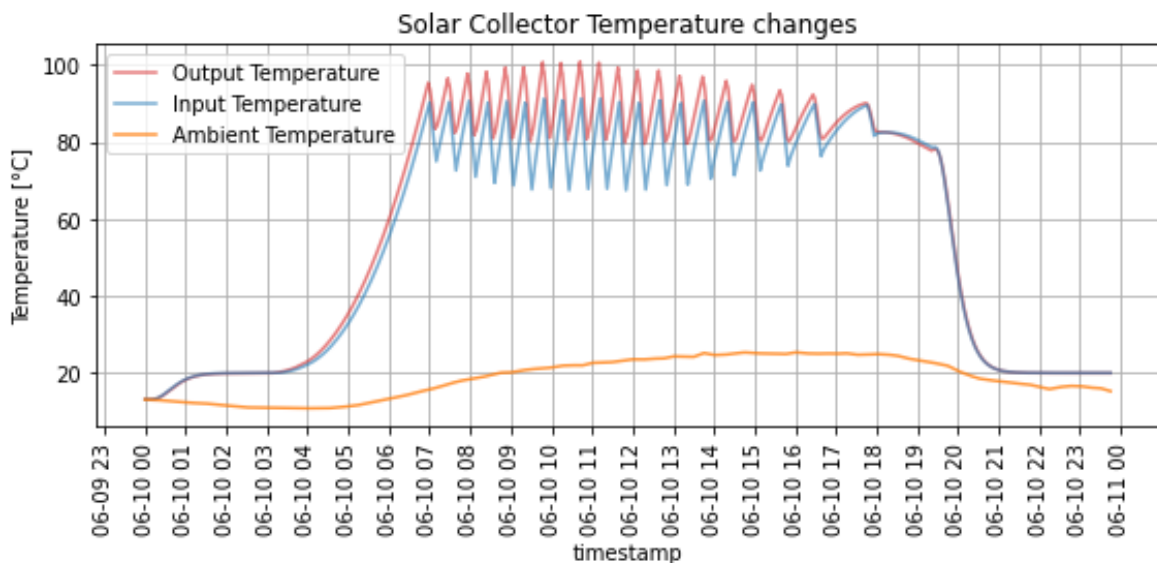


Figure 3.7 – Temperature changes in the solar collectors

The operational limits for the reversible heat pump are derived from the compressor manufacturer's datasheet, considering SHAKK's operating conditions. The temperature ranges for the refrigerant at the evaporator and condenser should ideally fall between -10°C and 10°C , and 10°C and 65°C , respectively. However, accounting for the assumed 5K temperature difference between the inflowing fluid and the refrigerant (explained in section 2.1.3), the specified temperature ranges for the inflowing temperatures into the compression chiller ($T_{in,cond}$ and $T_{in,evap}$) are as follows:

$$0^{\circ}\text{C} \leq T_{in,cond} \leq 55^{\circ}\text{C}$$

$$0^{\circ}\text{C} \leq T_{in,evap} \leq 20^{\circ}\text{C} \quad (\text{Eq.3-2})$$

$$T_{in,cond} - T_{in,evap} \geq 5^{\circ}\text{C}$$

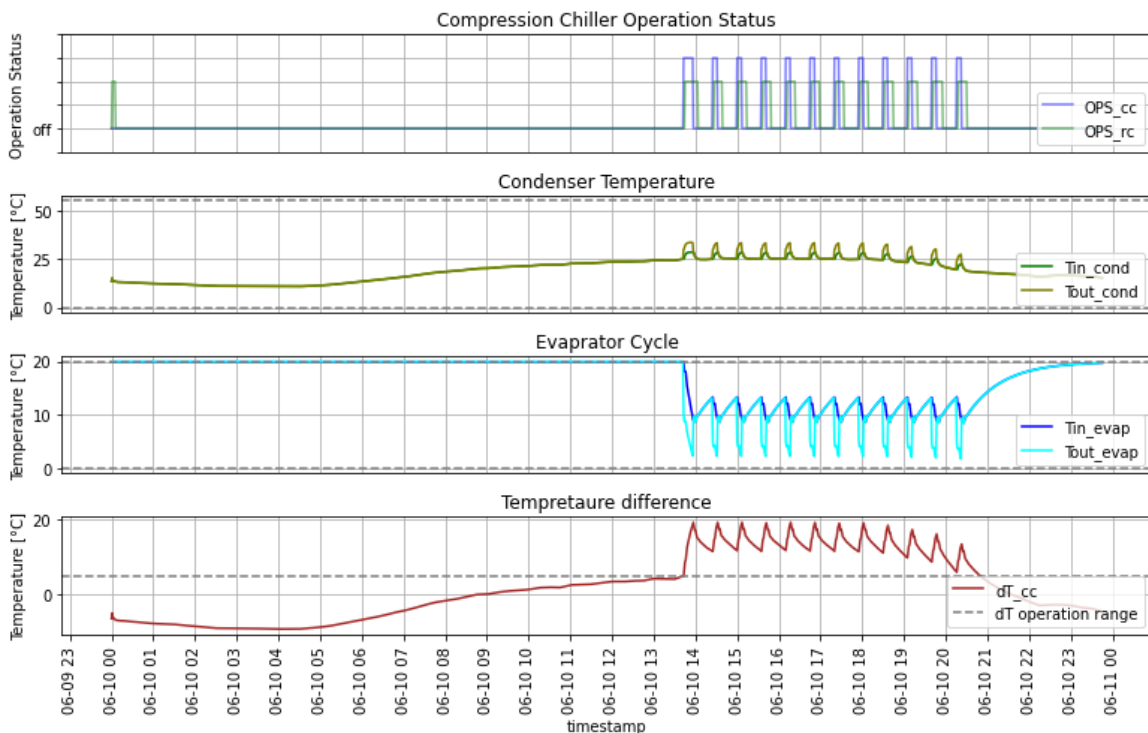


Figure 3.8 - Compression chiller's temperature changes

As a result, for the compression chiller to start cooling the cold storage, it requires an outdoor coil temperature above 25°C .

Figure 3.9 presents the cooling capacity, consumed electrical power, and COP of the chiller throughout the simulation. While the COP typically ranges between 2.5 and 6 for a typical compression chiller, the model exhibits a COP ranging from 5.69 to 8.58, with an average of 6.51. This deviation stems from the fact that the chiller

operates within a temperature range near the upper limit of its design. In spite of the model's COP values falling outside the typical range, the model's overall performance remains satisfactory, with the average Carnot efficiency² of the simulation at 31.9%, considered plausible despite potential errors due to limited training data.

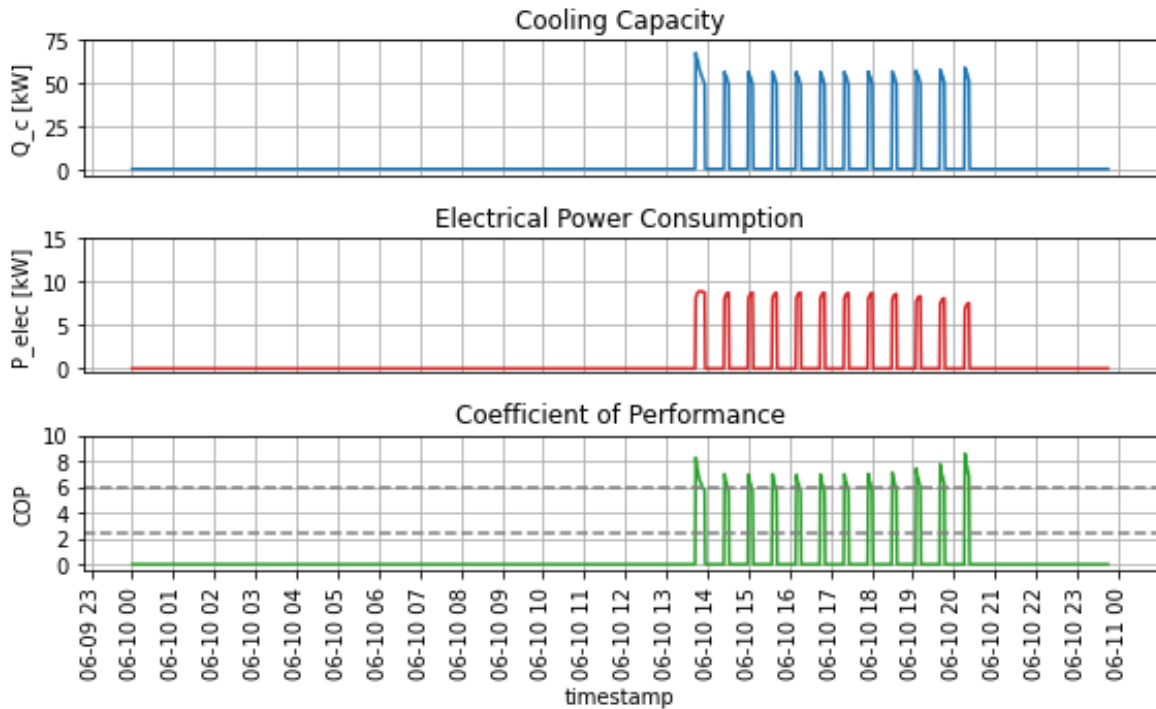


Figure 3.9 - Compression Chiller's COP changes

3.3 Heating via solar collectors

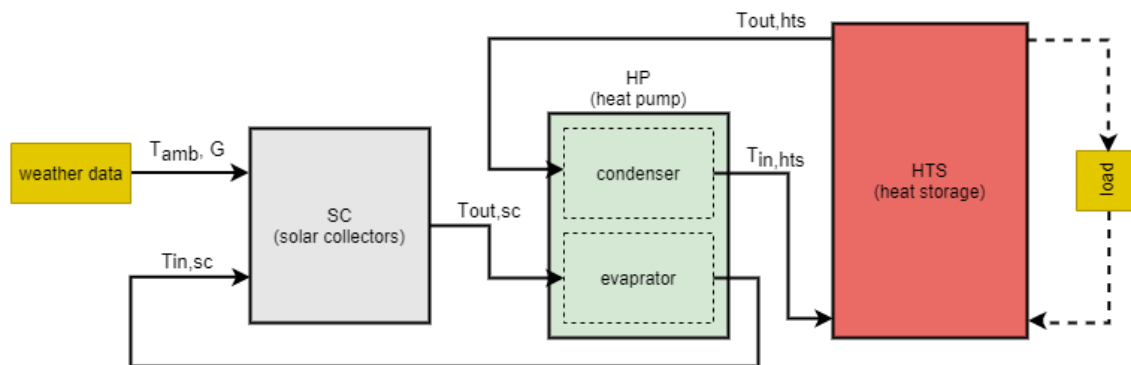


Figure 3.10 - Schematics of the data flow in heating via the solar collectors' operation mode

² Carnot efficiency represents the maximum possible efficiency that a heat engine can achieve operating between two temperature reservoirs and can be calculated as the ratio of the difference in temperature between the hot and cold reservoirs to the absolute temperature of the hot reservoir^[19].

In the heating operations, the reversible heat pump functions similarly to a conventional heat pump, as detailed in section 2.1.3. Figure 3.10 illustrates the data flow between components in this mode, while Table 3.3 outlines the volume flow rates between components.

For this simulation, the optimal day February 27, 2022, with maximum irradiance during the winter of 2021-22 was chosen. The day saw a peak total irradiance of about 630 W/m², with diffuse irradiance consistently higher than direct irradiance. Ambient temperatures fluctuated around 3°C until 6 a.m., gradually rising to a peak of slightly above 10°C in the afternoon before decreasing with a fairly constant slope to 4°C by day's end (Figure 3.11).

Table 3.3 - volume flow rates in between components

from	to	Volume flow rate [m ³ /h]
Solar collectors	Heat pump	6.0
Heat pump	Heat storage	8.5

At the start of the simulation, temperatures were assumed to match the ambient temperature, while the thermal storage was set at 20°C, with a constant load flow of 1m³/h at 20°C flowing into it from the bottom. The objective in heating simulation modes is to heat the water in the thermal storage to 55°C using the heat pump, with either the solar collectors or the outdoor coil providing the necessary heat. Figure 3.12 illustrates temperature trends in the solar collector during the simulation.

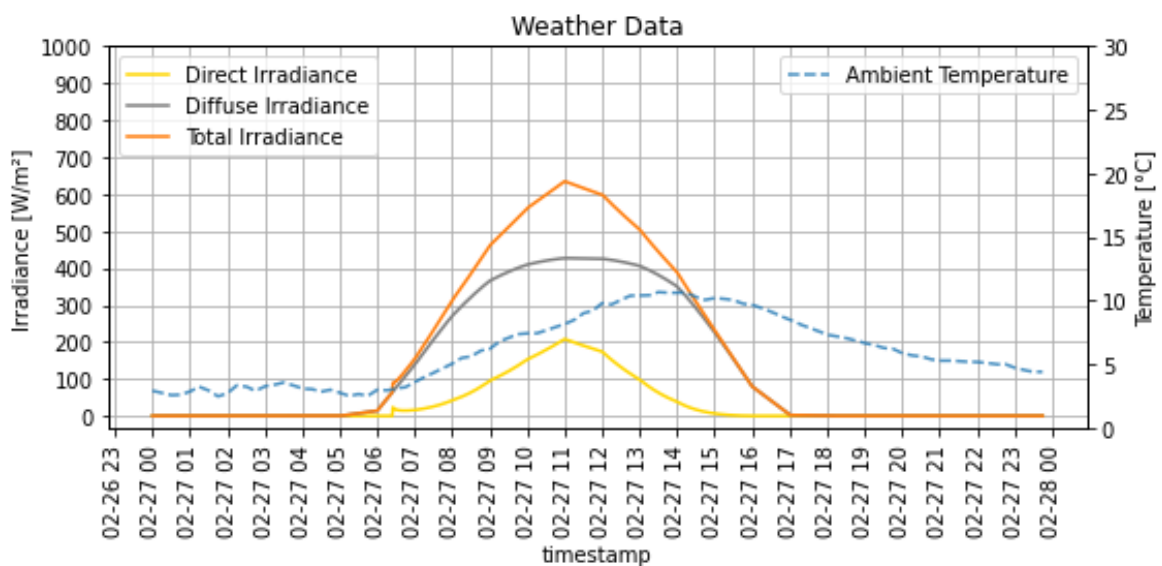


Figure 3.11 – Irradiance and temperature changes during the day 27.2.2022

It was noted that when the heat pump initiated operation, the temperature quickly dropped below ambient levels due to the heat pump's higher power relative to the collector's power in heating the transfer fluid. To ensure stability, a control mechanism was implemented to the heat pump, enforcing a minimum shutdown time of 10 minutes before reactivation. This allowed the solar collectors sufficient time to elevate the temperature in the evaporator's cycle. Nonetheless, the temperature in the solar collector circuit was below the ambient temperature for more than half the operation time.

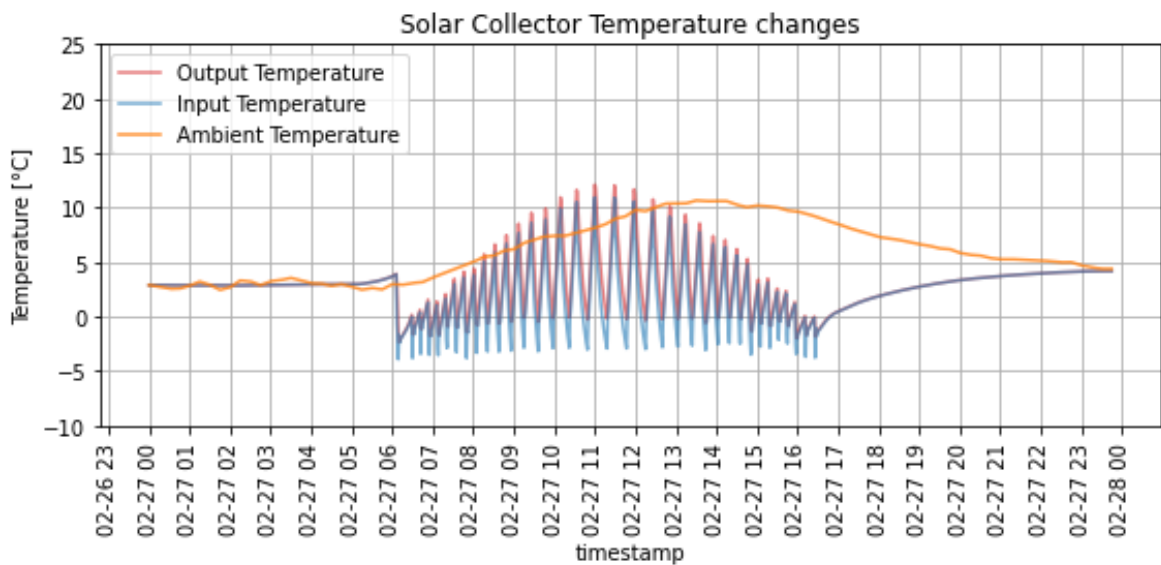


Figure 3.12 - Temperature changes in the solar collectors

Figure 3.13 illustrates the operational status of the heat pump and temperatures flowing in and out of the evaporator and condenser. The operational temperature limits for the heat pump remained consistent with those described previously. During the simulation, the heat pump stopped operating when the evaporator's inflow temperature fell below 0°C, turned on once temperatures returned within the designated range. However, the thermal storage temperature approached but never reached the target of 50°C.

Further analysis also revealed that on warmer days with equal or higher irradiance levels, such as in autumn, temperatures flowing into the evaporator from the solar collectors could exceed the upper temperature band. This could further restrict the operation conditions for heating via the solar collectors, as the collectors array was originally designed for cooling operations via the adsorption chiller.

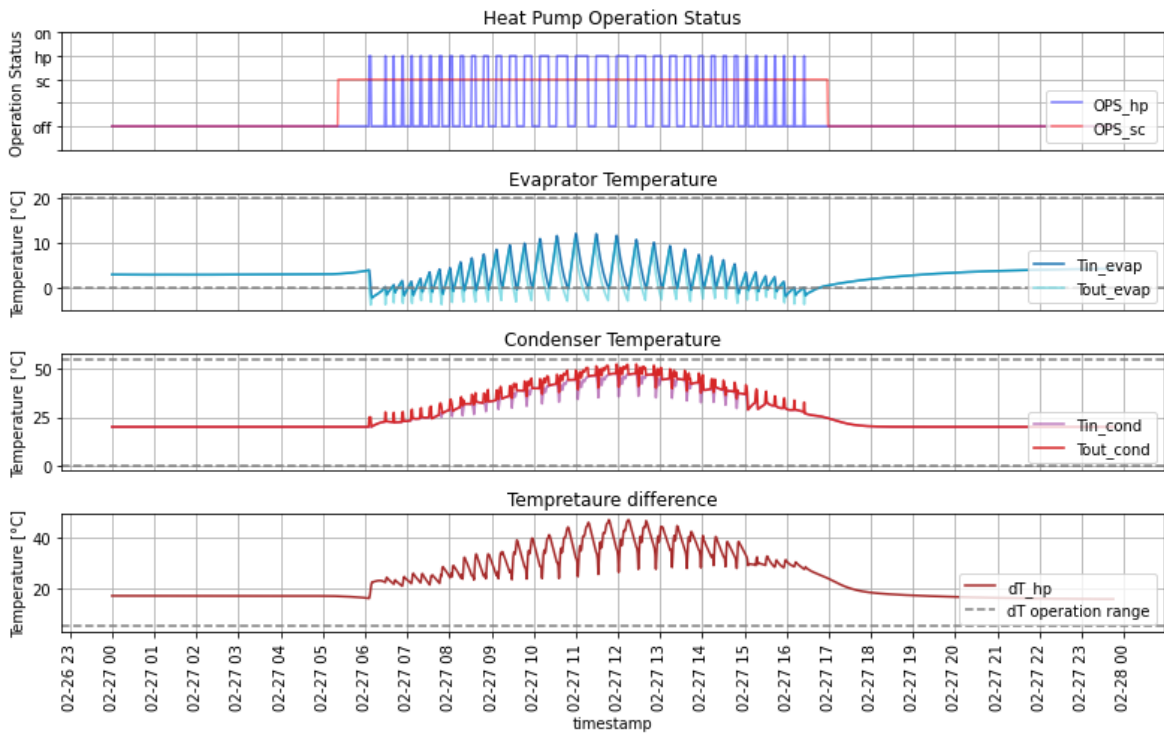


Figure 3.13 – Heat pump’s temperature changes

Evaluation of the heat pump model's performance is detailed in Figure 3.14, presenting COP changes throughout the simulation. Typically, a water-source heat pump exhibits a COP of 3 to 5. In our simulation, the average COP was 4.8, with an average Carnot efficiency of 56.6%, both of which are considered plausible results.

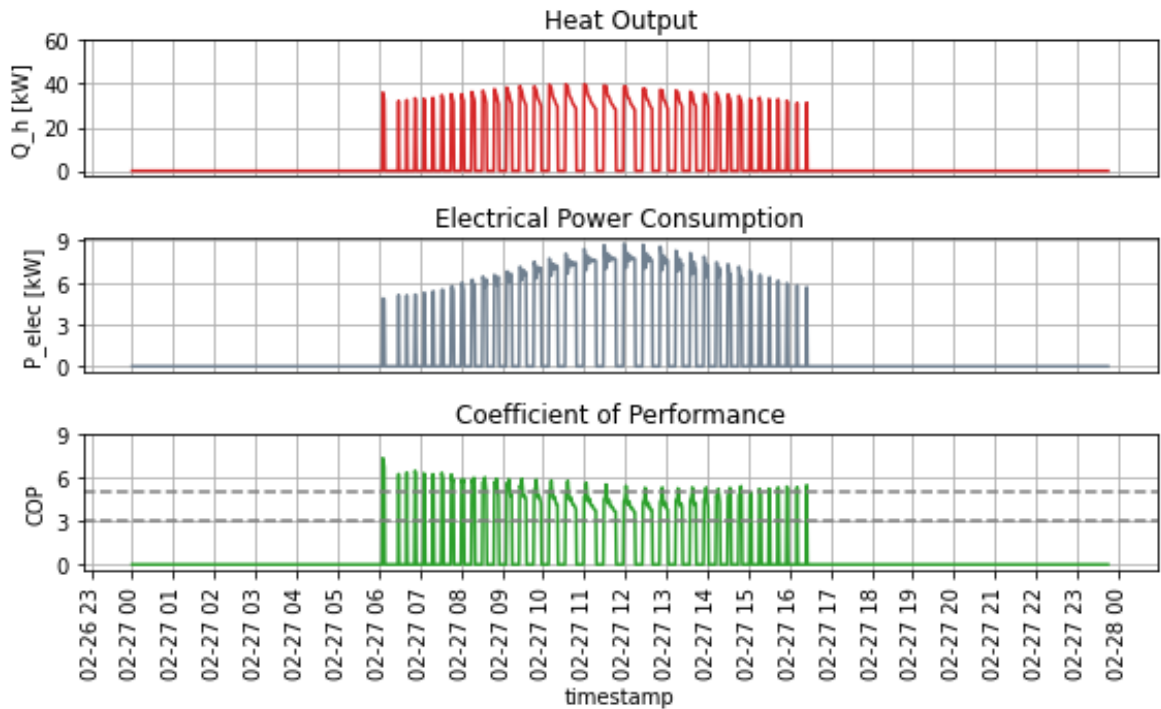


Figure 3.14 - Heat pump’s COP changes

3.4 Heating via outdoor coil

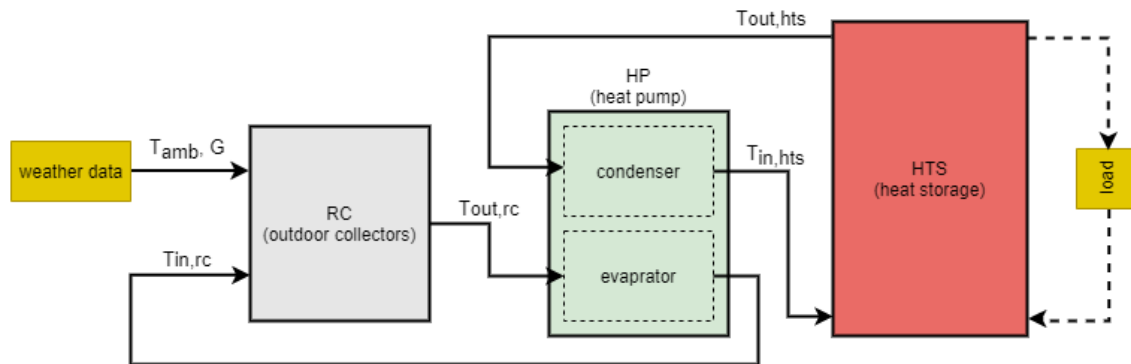


Figure 3.15 - Schematics of the data flow in heating via outdoor coil operation mode

Although this operation mode is typically intended for days with lower irradiance, the same date (27.2.2022) as used for heating via the solar collectors simulation was employed for this comparison. The initial conditions, including the temperatures at the outdoor coil, heat pump, and heat storage, as well as the constant load flow in the heat storage, control policies, and the volume flow rates (Table 3.4 - volume flow rates in between components) between the components, remain consistent across both simulation modes.

Table 3.4 - volume flow rates in between components

from	to	volume flow rate [m ³ /h]
Outdoor coil	Heat pump	6.0
Heat pump	Heat storage	8.5

The outdoor coil activates once the conditions for the heat pump are met and continues operating even after the heat pump stops until the circuit temperature returns to ambient levels. Figure 3.16 illustrates the temperature fluctuations in the heat pump.

Initially, significant oscillations occur from the start of the simulation until 8:30 a.m. This is due to the system operating close to the lower temperature limit of 0°C. During this period, the short operating cycles of the heat pump result in minimal temperature increase in the thermal storage, which remains at the same level as the constant load flow. However, as the ambient temperature rises later in the morning, these oscillations cease, marking a shift in the system's behavior. At this point, the

target temperature in the HTS is achieved and maintained within the desired range for the remainder of the day until the ambient temperature drops again at night.

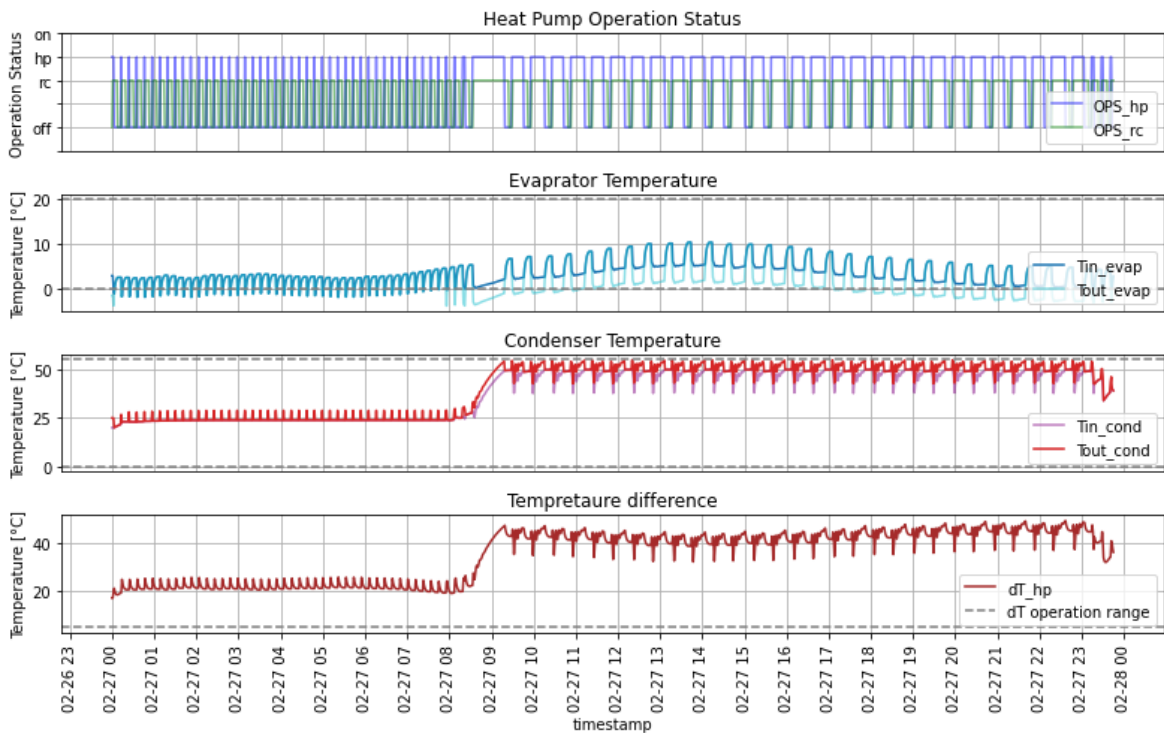


Figure 3.16 - Heat pump's temperature changes

The COP of the heat pump remains consistently above 6 for the first 8 and a half hours of the simulation. However, with the increase in ambient temperature during the day, it gradually decreases to between 3.5 and 5 for the duration of the simulation, as depicted in Figure 3.17. Throughout this simulation, the average COP was 3.84, with an average Carnot efficiency of 61%.

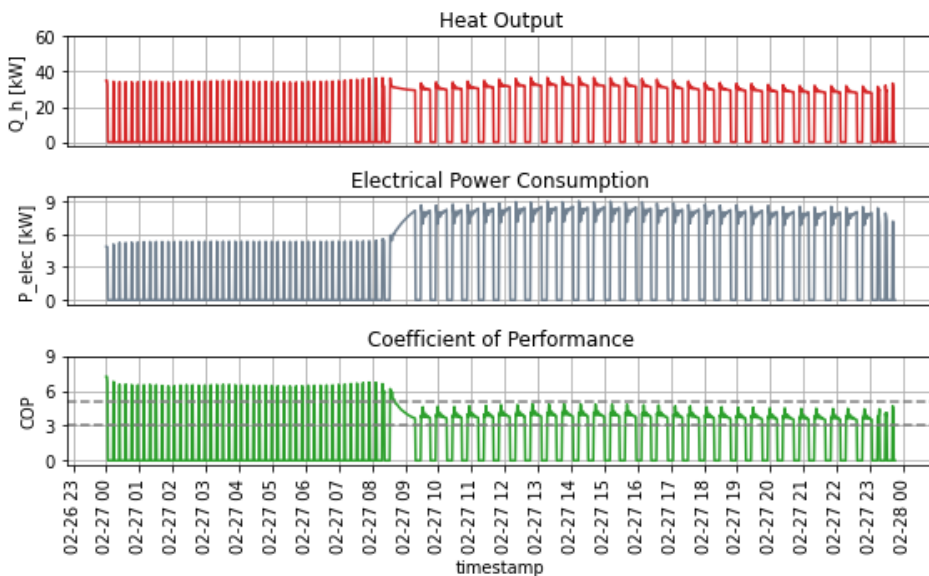


Figure 3.17 - Heat pump's COP changes

4 Summary and outlook

Chapter 2 provided a thorough exploration of the foundational principles guiding the modeling of each operational mode and individual components. In Chapter 3, a detailed analysis of the simulation results was presented. This chapter serves as a review, offering a condensed summary of the principal findings and outcomes for both cooling and heating operational modes. Furthermore, it explores potential paths for future research within each section. By revisiting the discoveries and outlining future research prospects, this chapter aims to provide a comprehensive understanding of the study's insights and pave the way for further investigations in the field.

Regarding the evaluation of the cooling modes, both configurations, involving solar collectors with an adsorption chiller and an outdoor coil with a compression chiller, were compared on a summer day with peak average irradiance. Results from simulations revealed that sufficient cooling could be provided by both setups throughout the day.

Additionally, since the operation of the adsorption chiller was more reliant on weather data, given that the energy for its operation was supplied by the solar collectors, one suggesting approach could be to develop a control strategy that would switch from the adsorption chiller to the compression chiller when solar irradiation falls below a certain threshold during the day. This adaptive approach will optimize system efficiency and reduce electricity consumption. Moreover, it was noted that both operation modes were sensitive to ambient temperatures below 25°C.

A potential solution is to introduce a pre-heating stage to the intermediate temperature circuit. This could be accomplished either by incorporating an external heat source or by routing the high-temperature circuit from the solar collectors to the intermediate temperature circuit. Such an enhancement will extend operation times and improve efficiency, particularly for the adsorption chiller system.

In the heating mode assessment, the operation of heating the heat storage using a heat pump was analyzed in two scenarios; one utilizing solar collectors as the heat pump's heat source, and the other utilizing the outdoor coil. It was observed that

heating via the outdoor coil demonstrated superior performance in terms of achieving and maintaining the target temperature within the desired range in the high temperature storage unit.

The decision to not prioritize running the heat pump via the solar collectors as the primary heating method is attributed to the narrow operational temperature band of the heat pump compared to that of the solar collectors. Originally designed to deliver high temperatures for the adsorption chiller, the solar collectors possess the capability to rapidly elevate temperature levels. However, if the heat pump initiates operation too early, especially in very cold ambient temperatures, rapid cycling may occur due to operation near the lower temperature limit. Conversely, if the heat pump starts operation slightly later or in warmer ambient conditions, it may exceed the upper temperature limit.

An alternative solution could involve connecting the heat pump and outdoor coil to the heat storage in parallel with the solar collectors, rather than solely relying on the heat pump in series connection with either the outdoor coil or the solar collectors. This configuration offers a greater potential for enhancing system performance. However, implementing this setup would necessitate a more intricate control policy.

Finally, there are several paths to enhance the accuracy and reliability of the simulation findings. One major aspect involves refining the regression model utilized for the reversible heat pump, which functions as both the compression chiller in the cooling cycle and the heat pump in the heating cycle. Integrating real-time measurement data for model training could significantly enhance the RHP model's precision, leading to more precise simulations. Additionally, incorporating a realistic load flow into the simulation framework would offer a more accurate portrayal of the system's behavior under diverse conditions. Moreover, extending the simulation duration beyond a single day could provide valuable insights into the system's long-term performance trends and dynamics, facilitating more comprehensive evaluations and optimizations.

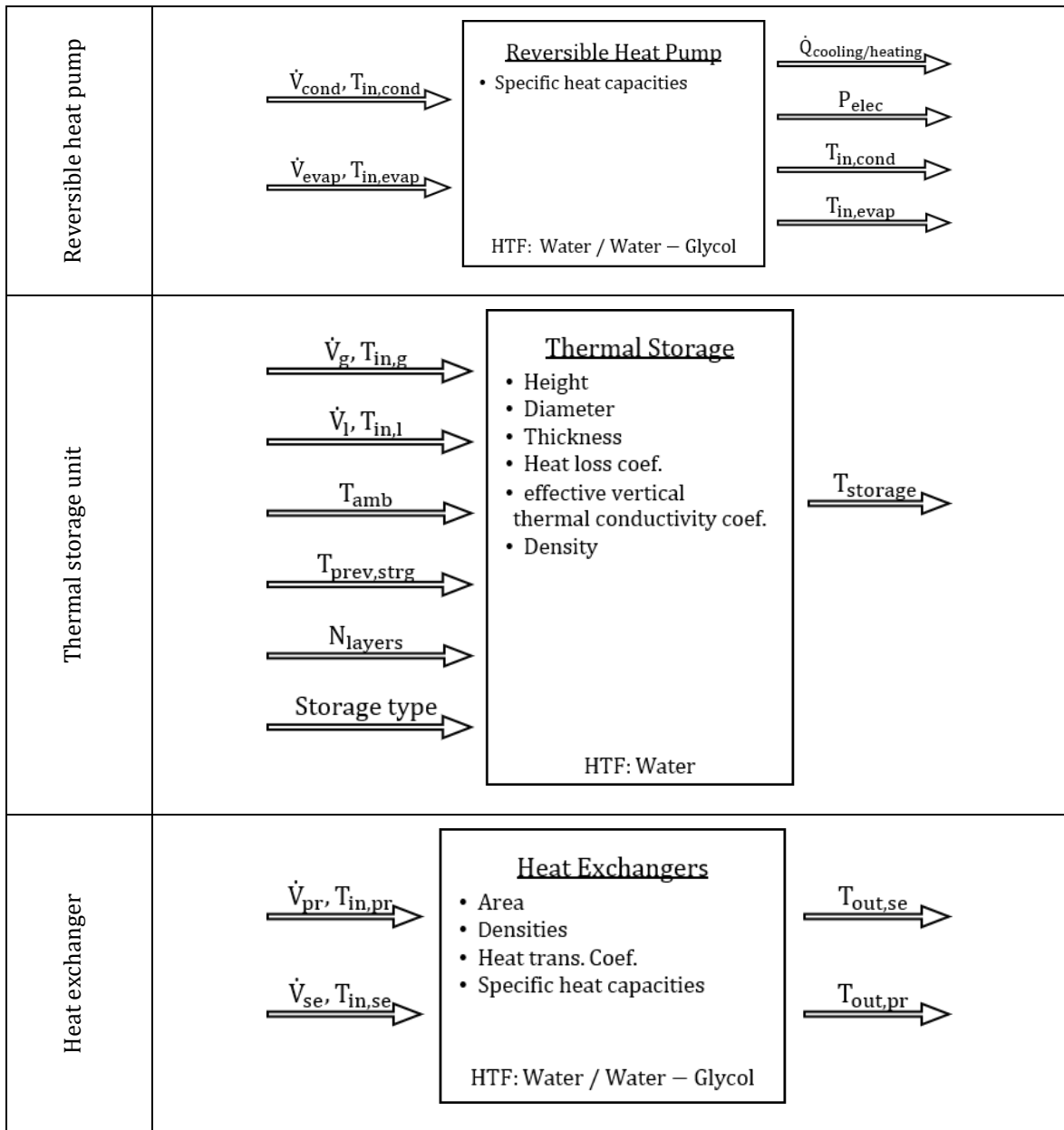
Bibliography

- [1] Energy generation. German Energy Solutions - Energy Generation. (n.d.). <https://www.german-energy-solutions.de/GES/Navigation/EN/Energy-Solutions/EnergyGeneration/energy-generation.html>
- [2] Bürger, A., Sawant, P. A., Wittstadt, U., Altmann-Dieses, A., & Pfafferott, J. (2022). Simulationsgestützte Systemauslegung für sorptionsgestützte, solare Kälteanlagen. *HLH: Lüftung, Klima, Heizung, Sanitär, Gebäudetechnik*, 73(4), 32-36.
- [3] Palomba, V., & Frazzica, A. (2021). Modeling of sorption systems for thermal energy storage. In *Advances in Thermal Energy Storage Systems* (pp. 453-475). Woodhead Publishing.
- [4] Python Software Foundation. (2024). Python 3.11 [Software]. Available from <https://www.python.org>
- [5] *Documentation*. scikit-learn. (n.d.). <https://scikit-learn.org/stable/#>
- [6] *Documentation*. pvlib python 0.10.4 documentation. (n.d.). <https://pvlib-python.readthedocs.io/en/stable/>
- [7] *Akotech GmbH*. AKOTEC Solarthermie. (n.d.). <https://www.akotec.eu/>
- [8] *Fahrenheit GmbH*. (n.d.). <https://fahrenheit.cool/en/>
- [9] Goel, M., Verma, V. S., & Tripathi, N. G. (2022). *Solar energy: Made simple for a sustainable future*. Springer.
- [10] ISO 9806:2017. (2022). Retrieved from <https://www.iso.org/standard/67978.html>
- [11] Solar Keymark Calculation Tool <https://solarkeymark.eu/wp-content/uploads/2021/10/Description-of-ScenoCalc-v6.1.pdf>
- [12] Henning, H., Motta, M. & Mugnier, D. (2013). *Solar Cooling Handbook: A Guide to Solar Assisted Cooling and Dehumidification Processes*. Berlin, Boston: Ambra Verlag. <https://doi.org/10.1515/9783990434390>
- [13] Wang, R., Wang, L., & Wu, J. (2014). *Adsorption Refrigeration Technology: Theory and application*. Wiley.
- [14] Sawant, P. A. (2021). A contribution to optimal scheduling of real-world trigeneration systems using economic model predictive control. Technische Universität Dresden.
- [15] Sawant, P., Bürger, A., Doan, M. D., Felsmann, C., & Pfafferott, J. (2020). Development and experimental evaluation of grey-box models of a microscale polygeneration system for application in optimal control. *Energy and Buildings*, 215, 109725.
- [16] Çengel, Y. A., & Ghajar, A. J. (2020). *Heat and mass transfer: Fundamentals & applications*. McGraw-Hill Education.
- [17] Mousavi Maleki, S. A., Hizam, H., & Gomes, C. (2017). Estimation of hourly, daily and monthly global solar radiation on inclined surfaces: Models re-visited. *Energies*, 10(1), 134.
- [18] Henning, H., Häberle, A., Lodi, A., & Motta, M. (2006, September). Solar cooling and refrigeration with high temperature lifts—thermodynamic background and technical solution. In *Proc. of 61st National ATI Congress, ATI-IIR International Session 'Solar Heating and Cooling'*, 14th September.
- [19] Çengel, Y. A., Boles, M. A., & Kanoglu, N. (2019). *Thermodynamics: An engineering approach*. McGraw-Hill.

Appendix

Data flow diagrams of individual components in SHAKK:

Component	Diagram
Solar collector array	<p style="text-align: center;">Solar Collector Array</p> <ul style="list-style-type: none"> • location • orientation • tilt • area • Efficiency • Specific heat capacity • Heat loss coef. • Effective thermal cap. <p style="text-align: center;">HTF: Water – Glycol</p>
Outdoor coil	<p style="text-align: center;">Dry Cooler / Outdoor Coil</p> <ul style="list-style-type: none"> • Heat transf. Area • Heat transf. Coef. • Specific heat capacities <p style="text-align: center;">HTF: Water – Glycol</p>
Adsorption chiller	<p style="text-align: center;">Adsorption Chiller</p> <ul style="list-style-type: none"> • Specific heat capacity <p style="text-align: center;">HTF: Water</p>



Thermal storage graphs in simulated operation modes

Mode	Component	Graph																																																																																																																																							
Cooling via AdC	HTS	<p>Thermal Storage Temperature Changes per Layer (HTS)</p> <table border="1"> <thead> <tr> <th>Timestamp</th> <th>level1 [°C]</th> <th>level2 [°C]</th> <th>level3 [°C]</th> <th>level4 [°C]</th> </tr> </thead> <tbody> <tr><td>06-09 23</td><td>13</td><td>13</td><td>13</td><td>13</td></tr> <tr><td>06-10 00</td><td>13</td><td>13</td><td>13</td><td>13</td></tr> <tr><td>06-10 01</td><td>13</td><td>13</td><td>13</td><td>13</td></tr> <tr><td>06-10 02</td><td>13</td><td>13</td><td>13</td><td>13</td></tr> <tr><td>06-10 03</td><td>13</td><td>13</td><td>13</td><td>13</td></tr> <tr><td>06-10 04</td><td>14</td><td>14</td><td>14</td><td>14</td></tr> <tr><td>06-10 05</td><td>20</td><td>20</td><td>20</td><td>20</td></tr> <tr><td>06-10 06</td><td>35</td><td>35</td><td>35</td><td>35</td></tr> <tr><td>06-10 07</td><td>75</td><td>75</td><td>75</td><td>75</td></tr> <tr><td>06-10 08</td><td>75</td><td>75</td><td>75</td><td>90</td></tr> <tr><td>06-10 09</td><td>75</td><td>75</td><td>75</td><td>90</td></tr> <tr><td>06-10 10</td><td>75</td><td>75</td><td>75</td><td>90</td></tr> <tr><td>06-10 11</td><td>75</td><td>75</td><td>75</td><td>90</td></tr> <tr><td>06-10 12</td><td>75</td><td>75</td><td>75</td><td>90</td></tr> <tr><td>06-10 13</td><td>75</td><td>75</td><td>75</td><td>90</td></tr> <tr><td>06-10 14</td><td>75</td><td>75</td><td>75</td><td>80</td></tr> <tr><td>06-10 15</td><td>75</td><td>75</td><td>75</td><td>75</td></tr> <tr><td>06-10 16</td><td>75</td><td>75</td><td>75</td><td>70</td></tr> <tr><td>06-10 17</td><td>75</td><td>75</td><td>75</td><td>75</td></tr> <tr><td>06-10 18</td><td>75</td><td>75</td><td>75</td><td>75</td></tr> <tr><td>06-10 19</td><td>75</td><td>75</td><td>75</td><td>75</td></tr> <tr><td>06-10 20</td><td>75</td><td>75</td><td>75</td><td>75</td></tr> <tr><td>06-10 21</td><td>75</td><td>75</td><td>75</td><td>75</td></tr> <tr><td>06-10 22</td><td>75</td><td>75</td><td>75</td><td>75</td></tr> <tr><td>06-10 23</td><td>75</td><td>75</td><td>75</td><td>75</td></tr> <tr><td>06-11 00</td><td>75</td><td>75</td><td>75</td><td>75</td></tr> </tbody> </table>	Timestamp	level1 [°C]	level2 [°C]	level3 [°C]	level4 [°C]	06-09 23	13	13	13	13	06-10 00	13	13	13	13	06-10 01	13	13	13	13	06-10 02	13	13	13	13	06-10 03	13	13	13	13	06-10 04	14	14	14	14	06-10 05	20	20	20	20	06-10 06	35	35	35	35	06-10 07	75	75	75	75	06-10 08	75	75	75	90	06-10 09	75	75	75	90	06-10 10	75	75	75	90	06-10 11	75	75	75	90	06-10 12	75	75	75	90	06-10 13	75	75	75	90	06-10 14	75	75	75	80	06-10 15	75	75	75	75	06-10 16	75	75	75	70	06-10 17	75	75	75	75	06-10 18	75	75	75	75	06-10 19	75	75	75	75	06-10 20	75	75	75	75	06-10 21	75	75	75	75	06-10 22	75	75	75	75	06-10 23	75	75	75	75	06-11 00	75	75	75	75
	Timestamp	level1 [°C]	level2 [°C]	level3 [°C]	level4 [°C]																																																																																																																																				
06-09 23	13	13	13	13																																																																																																																																					
06-10 00	13	13	13	13																																																																																																																																					
06-10 01	13	13	13	13																																																																																																																																					
06-10 02	13	13	13	13																																																																																																																																					
06-10 03	13	13	13	13																																																																																																																																					
06-10 04	14	14	14	14																																																																																																																																					
06-10 05	20	20	20	20																																																																																																																																					
06-10 06	35	35	35	35																																																																																																																																					
06-10 07	75	75	75	75																																																																																																																																					
06-10 08	75	75	75	90																																																																																																																																					
06-10 09	75	75	75	90																																																																																																																																					
06-10 10	75	75	75	90																																																																																																																																					
06-10 11	75	75	75	90																																																																																																																																					
06-10 12	75	75	75	90																																																																																																																																					
06-10 13	75	75	75	90																																																																																																																																					
06-10 14	75	75	75	80																																																																																																																																					
06-10 15	75	75	75	75																																																																																																																																					
06-10 16	75	75	75	70																																																																																																																																					
06-10 17	75	75	75	75																																																																																																																																					
06-10 18	75	75	75	75																																																																																																																																					
06-10 19	75	75	75	75																																																																																																																																					
06-10 20	75	75	75	75																																																																																																																																					
06-10 21	75	75	75	75																																																																																																																																					
06-10 22	75	75	75	75																																																																																																																																					
06-10 23	75	75	75	75																																																																																																																																					
06-11 00	75	75	75	75																																																																																																																																					
LTS	<p>Thermal Storage Temperature Changes per Layer (LTS)</p> <table border="1"> <thead> <tr> <th>Timestamp</th> <th>level1 [°C]</th> <th>level2 [°C]</th> <th>level3 [°C]</th> </tr> </thead> <tbody> <tr><td>06-09 23</td><td>20</td><td>20</td><td>20</td></tr> <tr><td>06-10 00</td><td>20</td><td>20</td><td>20</td></tr> <tr><td>06-10 01</td><td>20</td><td>20</td><td>20</td></tr> <tr><td>06-10 02</td><td>20</td><td>20</td><td>20</td></tr> <tr><td>06-10 03</td><td>20</td><td>20</td><td>20</td></tr> <tr><td>06-10 04</td><td>20</td><td>20</td><td>20</td></tr> <tr><td>06-10 05</td><td>20</td><td>20</td><td>20</td></tr> <tr><td>06-10 06</td><td>20</td><td>20</td><td>20</td></tr> <tr><td>06-10 07</td><td>20</td><td>20</td><td>20</td></tr> <tr><td>06-10 08</td><td>20</td><td>20</td><td>20</td></tr> <tr><td>06-10 09</td><td>20</td><td>20</td><td>20</td></tr> <tr><td>06-10 10</td><td>20</td><td>20</td><td>20</td></tr> <tr><td>06-10 11</td><td>20</td><td>20</td><td>20</td></tr> <tr><td>06-10 12</td><td>20</td><td>20</td><td>20</td></tr> <tr><td>06-10 13</td><td>20</td><td>20</td><td>20</td></tr> <tr><td>06-10 14</td><td>20</td><td>20</td><td>20</td></tr> <tr><td>06-10 15</td><td>10</td><td>10</td><td>10</td></tr> <tr><td>06-10 16</td><td>10</td><td>10</td><td>10</td></tr> <tr><td>06-10 17</td><td>10</td><td>10</td><td>10</td></tr> <tr><td>06-10 18</td><td>10</td><td>10</td><td>10</td></tr> <tr><td>06-10 19</td><td>15</td><td>15</td><td>15</td></tr> <tr><td>06-10 20</td><td>18</td><td>18</td><td>18</td></tr> <tr><td>06-10 21</td><td>19</td><td>19</td><td>19</td></tr> <tr><td>06-10 22</td><td>20</td><td>20</td><td>20</td></tr> <tr><td>06-10 23</td><td>20</td><td>20</td><td>20</td></tr> <tr><td>06-11 00</td><td>20</td><td>20</td><td>20</td></tr> </tbody> </table>	Timestamp	level1 [°C]	level2 [°C]	level3 [°C]	06-09 23	20	20	20	06-10 00	20	20	20	06-10 01	20	20	20	06-10 02	20	20	20	06-10 03	20	20	20	06-10 04	20	20	20	06-10 05	20	20	20	06-10 06	20	20	20	06-10 07	20	20	20	06-10 08	20	20	20	06-10 09	20	20	20	06-10 10	20	20	20	06-10 11	20	20	20	06-10 12	20	20	20	06-10 13	20	20	20	06-10 14	20	20	20	06-10 15	10	10	10	06-10 16	10	10	10	06-10 17	10	10	10	06-10 18	10	10	10	06-10 19	15	15	15	06-10 20	18	18	18	06-10 21	19	19	19	06-10 22	20	20	20	06-10 23	20	20	20	06-11 00	20	20	20																												
Timestamp	level1 [°C]	level2 [°C]	level3 [°C]																																																																																																																																						
06-09 23	20	20	20																																																																																																																																						
06-10 00	20	20	20																																																																																																																																						
06-10 01	20	20	20																																																																																																																																						
06-10 02	20	20	20																																																																																																																																						
06-10 03	20	20	20																																																																																																																																						
06-10 04	20	20	20																																																																																																																																						
06-10 05	20	20	20																																																																																																																																						
06-10 06	20	20	20																																																																																																																																						
06-10 07	20	20	20																																																																																																																																						
06-10 08	20	20	20																																																																																																																																						
06-10 09	20	20	20																																																																																																																																						
06-10 10	20	20	20																																																																																																																																						
06-10 11	20	20	20																																																																																																																																						
06-10 12	20	20	20																																																																																																																																						
06-10 13	20	20	20																																																																																																																																						
06-10 14	20	20	20																																																																																																																																						
06-10 15	10	10	10																																																																																																																																						
06-10 16	10	10	10																																																																																																																																						
06-10 17	10	10	10																																																																																																																																						
06-10 18	10	10	10																																																																																																																																						
06-10 19	15	15	15																																																																																																																																						
06-10 20	18	18	18																																																																																																																																						
06-10 21	19	19	19																																																																																																																																						
06-10 22	20	20	20																																																																																																																																						
06-10 23	20	20	20																																																																																																																																						
06-11 00	20	20	20																																																																																																																																						

Mode	Component	Graph
Cooling via CC	HTS	<p>Thermal Storage Temperature Changes per Layer</p>
	LTS	<p>Thermal Storage Temperature Changes per Layer</p>

Mode	Component	Graph
Heating via SC	LTS	<p>Thermal Storage Temperature Changes per Layer</p> <p>Temperature [°C]</p> <p>level1 level2 level3 level4</p> <p>timestamp</p>
Heating via OC	LTS	<p>Thermal Storage Temperature Changes per Layer</p> <p>Temperature [°C]</p> <p>level1 level2 level3 level4</p> <p>timestamp</p>

Solar Keymarks data sheet



Precisely Right.

Annex to Solar Keymark Certificate							Licence Number		011-752827 R			
							Date issued		2019-02-01			
							Issued by		TÜV Rheinland Energy GmbH			
Licence holder	Ako Tec Produktionsgesellschaft						Country	Germany				
Brand (optional)	Ako Tec						Web	www.akotec.eu				
Street, Number	Grundmühlenweg 3						E-mail	info@akotec.eu				
Postcode, City	16278 Angermünde						Tel	+49 (0)3331 25 716 30				
Collector Type	Evacuated tubular collector											
Collector name	Gross height mm	Gross area (A _g) m ²	Gross length h mm	Gross width s mm	Aperture area (A _a) m ²		Power output per collector G _b = 850 W/m ² , G _d = 150 W/m ² & u = 1.3 m/s θ _m - θ _a					
							0 K W	10 K W	30 K W	50 K W	70 K W	100 K W
MEGA-Kollektor Segment mit 26Röhren	159	4.33	1983	2184	3.87	2122	2095	2040	1985	1930	1848	
MEGA-Kollektor Segment mit 78Röhren	159	12.99	5950	2184	11.60	6365	6283	6119	5954	5790	5543	
Power output per m ² gross area							490	484	471	458	446	427
Performance parameters test method	Quasi dynamic											
Performance parameters (related to A ₀)	η _{0, b}	a1	a2	a3	a4	a5	a6	a7	a8	Kd		
Units	-	W/(m ² K)	W/(m ² K ²)	J/(m ² K)	-	J/(m ² K)	s/m	W/(m ² K ⁴)	W/(m ² K ⁴)	-		
Test results	0.483	0.63	0.000	0.000	0.00	8.136	0.000	0.00	0.0E+00	1.10		
Incidence angle modifier test method	Quasi dynamic - outdoor											
Incidence angle modifier	Angle	10°	20°	30°	40°	50°	60°	70°	80°	90°		
Transversal	K _{θT, coll}	1.24	1.25	1.29	1.08	1.23	1.18	1.15	0.97	0.00		
Longitudinal	K _{θL, coll}	1.00	1.00	0.99	0.98	0.97	0.94	0.89	0.44	0.00		
Heat transfer medium for testing	Water											
Flow rate for testing (per gross area, A _g)	dm/dt	0.036 kg/(sm ²)										
Maximum temperature difference during thermal performance test	(θ _m -θ _a) _{max}	70 K										
Standard stagnation temperature (G = 1000 W/m ² ; θ _a = 30 °C)	θ _{stg}	170 °C										
Maximum operating temperature	θ _{max, op}	180 °C										
Maximum operating pressure	p _{max, op}	1000 kPa										
Testing laboratory	TÜV Rheinland Energy GmbH						www.tuv.com/solarpower					
Test report(s)	21242732.001rev1						Dated	01.02.2019				
Comments of testing laboratory	The results related to aperture area (as listed above) and hemispherical efficiency with 85% beam and 15 % diffuse irradiance at normal incidence are: h _{0, hem, a} = 0.549; a _{1, a} = 0.704; a _{2, a} = 0.000						Datasheet version: 6.0, 2018-10-30					
 TÜV Rheinland Energy GmbH Am Grauen Stein 51105 Köln												
DIN CERTCO • Alboinstraße 56 • 12103 Berlin, Germany Tel: +49 30 7562-1131 • Fax: +49 30 7562-1141 • E-Mail: info@dincertco.de • www.dincertco.de												

Annex to Solar Keymark Certificate		Licence Number												
Supplementary Information		011-752827 R												
		Issued												
		2019-02-01												
Annual collector output in kWh/collector at mean fluid temperature $\bar{\theta}_m$														
	Standard Locations	Athens			Davos			Stockholm			Würzburg			
Collector name	$\bar{\theta}_m$	25°C	50°C	75°C	25°C	50°C	75°C	25°C	50°C	75°C	25°C	50°C	75°C	
MEGA-Kollektor Segment mit 26 Röhren		4 185	3 904	3 640	3 698	3 433	3 191	2 654	2 418	2 216	2 831	2 583	2 363	
MEGA-Kollektor Segment mit 78 Röhren		12 551	11 709	10 919	11 090	10 297	9 571	7 959	7 252	6 647	8 492	7 746	7 088	
Annual output per m ² gross area		966	901	841	854	793	737	613	558	512	654	596	546	
Fixed or tracking collector		Fixed (slope = latitude - 15°; rounded to nearest 5°)												
Annual irradiation on collector plane		1765 kWh/m ²			1714 kWh/m ²			1166 kWh/m ²			1244 kWh/m ²			
Mean annual ambient air temperature		18.5°C			3.2°C			7.5°C			9.0°C			
Collector orientation or tracking mode		South, 25°			South, 30°			South, 45°			South, 35°			
The collector is operated at constant temperature $\bar{\theta}_m$ (mean of in- and outlet temperatures). The calculation of the annual collector performance is performed with the official Solar Keymark spreadsheet tool Scenocalc Ver. 6.0 (October 2018). A detailed description of the calculations is available at www.solarkeymark.org/scenocalc														
Additional Information														
Collector heat transfer medium		Water-Glycole												
The collector is deemed to be suitable for roof integration		No												
The collector was tested successfully under the following conditions:														
Climate class (A+, A, B or C)		A												
G (W/m ²) >	1000	$\bar{\theta}_a$ (°C) >			20	H _x (MJ/m ²) >			600					
Maximum tested positive load								3000			Pa			
Maximum tested negative load								2000			Pa			
Hail resistance using steel ball (maximum drop height)								35			m			
Additional collector attribute(s)														
<input type="checkbox"/> Using external power source(s) for normal operation		<input type="checkbox"/> Active or passive measure(s) for self-protection												
<input type="checkbox"/> Co-generating thermal and electrical power		<input type="checkbox"/> Wind and/or infrared sensitive collector(s) (WISC)												
<input type="checkbox"/> Façade collector(s)														
Energy Labelling Information														
	Reference Area, A _{ref} (m ²)	Hydraulic Designation Code												
MEGA-Kollektor Segment mit 26 Röhren	4.33	1-H-12S-C:64,1983												
MEGA-Kollektor Segment mit 78 Röhren	12.99	1-H-12S-C:64,5949												
Data required for CDR (EU) No 811/2013 - Reference Area A_{ref}														
Collector efficiency (η_{col})	46%	Data required for CDR (EU) No 812/2013 - Reference Area A_{ref}												
Remark: Collector efficiency (η_{col}) is defined in CDR (EU) No 811/2013 as collector efficiency of the solar collector at a temperature difference between the solar collector and the surrounding air of 40 K and a global solar irradiance of 1000 W/m ² , expressed in % and rounded to the nearest integer. Deviating from the regulation η_{col} is based on reference area (A _{ref}) which is aperture area for values according to EN 12975-2 or gross area for ISO 9806:2017.		Zero-loss efficiency (η_0)	0.49	--										
		First-order coefficient (a ₁)	0.63	W/(m ² K)										
		Second-order coefficient (a ₂)	0.000	W/(m ² K ²)										
		Incidence angle modifier IAM (50°)	1.06	--										
		Remark: The data given in this section are related to collector reference area (A _{ref}) which is aperture area for values according to EN 12975-2 or gross area for ISO 9806. Consistent data sets for either aperture or gross area can be used in calculations like in the regulation 811 and 812 and simulation programs.												
DIN CERTCO • Alboinstraße 56 • 12103 Berlin, Germany														
Tel: +49 30 7562-1131 • Fax: +49 30 7562-1141 • E-Mail: info@dincertco.de • www.dincertco.de														

Reversible heat pump datasheet

Reversible heat pump operation limits:

HG34e/380-4 S HC

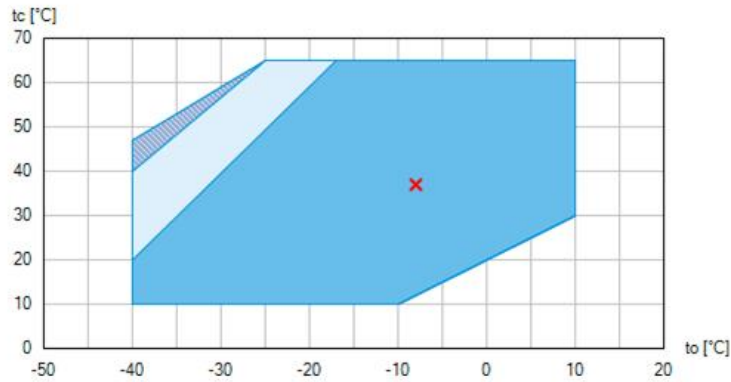
Engine: 220-240V Δ /380-420V Y -3- 50Hz




Refrigerant: R290

Subject:

BOCK colour the world of tomorrow

Operating limits



-  Discharge end temperature min. 20K above condensing temperature (dew point)
-  Supplementary cooling or reduced suction gas temperature ($\Delta t_{oh} < 20K$)
-  Supplementary cooling and reduced suction gas temperature ($\Delta t_{oh} < 20K$)

The compressor can be operated within the limits of the applications shown in the diagram. Please note the importance of the colour shaded areas.

In the dark blue range the discharge end temperature has to be at least 20K above the condensing temperature (dew point).

An internal IHX heat exchanger must be provided for this if necessary.

Thresholds should not be selected as the design point or the continuous operating point.

Subject to change without notice

To:

From:

08.11.2022
Page 2 of 10

VAP 11.12.2

Data used for training of the heat pump's regression model:

HG34e/380-4 S HC

Engine: 220-240V Δ/ 380-420V Y -3- 50Hz

Refrigerant: R290

Subject:



Performance data table

Application: Heat Pump

Reference temperature: Dew point

Compressor frequency: 50 Hz ¹⁾




Voltage: 400 V

Suction gas temperature: 20 °C

Subcooling (outside cond.): 0 K

tc [°C]		to [°C]									
		0.0	-5.0	-10.0	-15.0	-20.0	-25.0	-30.0	-35.0	-40.0	
30.0	Q [W]	31800	27300	23200	19500	16200	13300	10600	8320	6360	
	P [kW]	5.27	5.20	5.02	4.74	4.39	3.99	3.55	3.11	2.68	
35.0	Q [W]	31100	26700	22700	19100	15900	12900	10400	8050	6080	
	P [kW]	5.86	5.69	5.42	5.06	4.63	4.15	3.66	3.16	2.68	
40.0	Q [W]	30200	26000	22100	18600	15400	12600	10000	7750	5790	
	P [kW]	6.42	6.16	5.80	5.35	4.85	4.31	3.75	3.19	2.67	
45.0	Q [W]	29300	25200	21500	18100	15000	12200	9640	7430	5480	
	P [kW]	6.97	6.61	6.16	5.64	5.06	4.45	3.83	3.22	2.65	
50.0	Q [W]	28300	24400	20700	17400	14400	11700	9250	7070		
	P [kW]	7.49	7.05	6.51	5.91	5.26	4.59	3.91	3.25		

The performance data are preliminary, computed values. Variations, however, cannot be excluded.

-  Supplementary cooling or reduced suction gas temperature ($\Delta t_{oh} < 20K$)
-  Supplementary cooling and reduced suction gas temperature ($\Delta t_{oh} < 20K$)
-  Max. compressor frequency exceeded.

to Evaporating temperature
 tc Condensing temperature
 Q Heating capacity (incl. subcooling)
 P Power consumption

1) Selection and operation of compressors with external frequency inverter (third-party product):
 For the released frequency range of the Bock compressor, see technical data or at min./max. cooling capacity.
 The maximum permissible working current of the compressor ($I_{max,comp}$) (see technical data) must not be exceeded. If abnormal vibrations occur in the system, the affected frequency ranges has to be blanked out in the frequency converter accordingly.
 The maximum output current of the frequency converter must be greater than $I_{max,comp}$. For a safe start of the compressor, the frequency converter, for applications with low pressure refrigerants HP up to 28 bar, must be able to supply a short-term overload of min. 140% of $I_{max,comp}$ for min. 3 seconds. For applications with high pressure refrigerants (e.g. CO₂) a value of min. 160% of $I_{max,comp}$ for min. 3 sec has to be supplied.
 Carry out all designs and installations in accordance with local safety regulations and common regulations (e.g. VDE), as well as the specifications of the frequency inverter manufacturer.

Notes regarding capacity data:
 When compressor is operated with frequency inverter the capacity data is calculated out of the 50Hz-data and is intended as an assistance to determine the capacity data at different frequencies. Deviations cannot be excluded.

Subject to change without notice

To:

From:

08.11.2022
 Page 5 of 10

VAP 11.12.2

Data used for training of the compression chiller's regression model:

HG34e/380-4 S HC

Motor: 220-240V Δ/ 380-420V Y -3- 50Hz
Kältemittel: R290

GEA Commercial Compressors



Betreff:

Tabelle Leistungsdaten

Anwendung: Kälte- und Klimaanlage
Bezugstemperatur: Taupunkt
Verdichterfrequenz: 69 Hz ¹⁾
Spannung: 400 V
Sauggasüberhitzung: 20 K
Unterkühlung (außerh. Verfl.): 9 K

tc [°C]		to [°C]									
		0,0	-5,0	-10,0	-15,0	-20,0	-25,0	-30,0	-35,0	-40,0	
30,0	Q [W]	38000	31600	25900	20900	16700	13000	9840	7240	5080	
	P [kW]	7,54	7,44	7,18	6,78	6,28	5,70	5,08	4,45	3,84	
35,0	Q [W]	36300	30100	24600	19900	15800	12300	9280	6770	4680	
	P [kW]	8,38	8,14	7,75	7,23	6,62	5,94	5,23	4,52	3,83	
40,0	Q [W]	34400	28500	23300	18800	14900	11600	8690	6290	4280	
	P [kW]	9,18	8,81	8,29	7,66	6,94	6,16	5,36	4,57	3,81	
45,0	Q [W]	32500	26900	21900	17700	14000	10800	8070	5790	3860	
	P [kW]	9,96	9,46	8,81	8,06	7,24	6,37	5,48	4,61	3,78	
50,0	Q [W]	30400	25100	20400	16400	12900	9920	7390	5240		
	P [kW]	10,70	10,00	9,32	8,45	7,53	6,56	5,59	4,65		

Bei den angegebenen Leistungsdaten handelt es sich um rechnerisch ermittelte, vorläufige Werte. Abweichungen können daher nicht ausgeschlossen werden. Bitte beachten Sie die Hinweise zur Sauggasüberhitzung.

- Zusatzkühlung oder reduzierte Sauggastemperatur ($\Delta t_{oh} < 20K$)
- Zusatzkühlung und reduzierte Sauggastemperatur ($\Delta t_{oh} < 20K$)
- Die maximal mögliche Verdichterfrequenz ist überschritten

to Verdampfungstemperatur
tc Verflüssigungstemperatur
Q Verdichterkälteleistung
P Leistungsaufnahme

- 1) Auswahl und Betrieb von Verdichtern mit externem Frequenzumformer (Fremdfabrikat):
Freigegebener Frequenzbereich des GEA Bock Verdichters siehe technische Daten in der Montageanleitung bzw. in der Software bei min./max. Kälteleistung.
Der maximal zulässige Betriebsstrom des Verdichters ($I_{max, Verdichter}$) (siehe Typschild oder technische Daten) darf nicht überschritten werden. Bei auftretenden abnormalen Schwingungen in der Anlage müssen die betroffenen Frequenzbereiche im Frequenzumformer entsprechend ausblendet werden.
Der maximale Ausgangsstrom des Frequenzumformers muss größer sein als $I_{max, Verdichter}$.
Zum sicheren Start des Verdichters muss der Frequenzumformer, bei Anwendungen mit Niederdruckkältemittel HD bis 28 bar, für min. 3 Sekunden eine kurzzeitige Überlast von min. 140% des $I_{max, Verdichter}$ aufbringen können.
Bei Anwendungen mit Hochdruckkältemittel (z. B. CO₂) gilt ein Wert von min. 160% des $I_{max, Verdichter}$ ebenfalls für min. 3 Sekunden.
Führen Sie alle Auslegungen und Installationen gemäß den örtlichen Sicherheitsbestimmungen und gängigen Vorschriften (z.B. VDE), sowie gemäß den Angaben des Frequenzumformerherstellers aus.

Hinweise zu den Leistungsdaten:

Die Leistungsdaten im Betrieb mit Frequenzumformer werden aus den 50Hz-Daten berechnet und dienen als Hilfestellung zur Ermittlung der zu erwartenden Leistungsdaten bei unterschiedlichen Frequenzen. Abweichungen können nicht ausgeschlossen werden.

Änderungen vorbehalten

An:

Von:

09.06.2020
Seite 4 von 8

VAP 11.5.10 (win)